

# The Behavior of the Lithosphere on Seismic to Geologic Timescales

A.B. Watts,<sup>1</sup> S.J. Zhong,<sup>2</sup> and J. Hunter<sup>1</sup>

<sup>1</sup>Department of Earth Sciences, University of Oxford, OX1 3AN, United Kingdom; email: tony@earth.ox.ac.uk

<sup>2</sup>Department of Physics, University of Colorado, Boulder, Colorado 80309

Annu. Rev. Earth Planet. Sci. 2013. 41:443–68

The *Annual Review of Earth and Planetary Sciences* is online at earth.annualreviews.org

This article's doi:  
10.1146/annurev-earth-042711-105457

Copyright © 2013 by Annual Reviews.  
All rights reserved

## Keywords

elastic thickness, viscosity, flexure, stress relaxation, rheology

## Abstract

The strength of the lithosphere and how it responds to loading and unloading are fundamental problems with wide implications. Flexure studies suggest that the elastic thickness, a proxy for the strength of the lithosphere, increases with plate age but decreases with load age. The elastic thickness is significantly less than the seismic thickness of the lithosphere, as indicated by the depth to the low-velocity zone, suggesting that the lithosphere is a strong structure at short seismic timescales and a weak one at long timescales. The mechanism controlling this weakening is not known, but it probably involves some form of load-induced stress relaxation. Despite weakening, the lithosphere is capable of retaining its strength and supporting loads such as volcanoes and sediments for long periods of geological time. Lithosphere relaxation should be included in geodynamical models, especially as it has impacts on stratigraphy, sea-level change, and dynamic topography.

## 1. INTRODUCTION

The Earth's lithosphere responds to the forces imposed on it during, for example, subduction and orogeny and continental breakup and rifting by continuously deforming. The deformation is manifest in geological and geophysical observations such as the structural styles in orogens, the stratigraphic "architecture" of sedimentary basins, and the large-scale geometry of the crust and uppermost mantle. The nature of the deformation, particularly its spatial and temporal scales, places constraints on the lithosphere's physical properties, which, in turn, have implications for sedimentary basins, sea-level change, and dynamic topography.

Unfortunately, there are few tectonic settings on Earth where the deformation can be studied over sufficiently large spatial and temporal scales. The only evidence we have are "snapshots" of the response to different types of loads at particular temporal and spatial scales (e.g., **Figure 1**). Examples include the response that follows earthquake triggering (e.g., Nishimura & Thatcher 2003, Motagh et al. 2006); the waxing and waning of ice sheets and glacial lakes (e.g., Peltier 2002, Latychev et al. 2005); and lithospheric flexure due to sediment, volcano, and orogenic loading (e.g., Watts 2001). These snapshots involve temporal scales that range from a few seconds to several tens of millions of years and spatial scales from a few kilometers to several hundreds of kilometers, each of which indicates a different rheological structure (**Figure 1**).

Of all the snapshots, flexure involves the largest displacements (up to a few kilometers) and, potentially, the greatest range of loading and unloading times (up to  $10^9$  yr). Flexure, like all isostatic models, however, is an idealized state that Earth's crust and upper mantle tend toward when disturbed by loading or unloading. For example, since the pioneering works of Joseph Barrell and Ross Gunn, we have known that Earth's lithosphere can be both weak and strong and may either promote or resist deformation, but we know little about the timescales over which isostatic adjustment operates and about whether the lithosphere, like its underlying asthenosphere, undergoes a relaxation. Nevertheless, flexural isostasy is one of only a few lines of evidence on the physical properties of the lithosphere, such as its rigidity, which can be examined in relation to

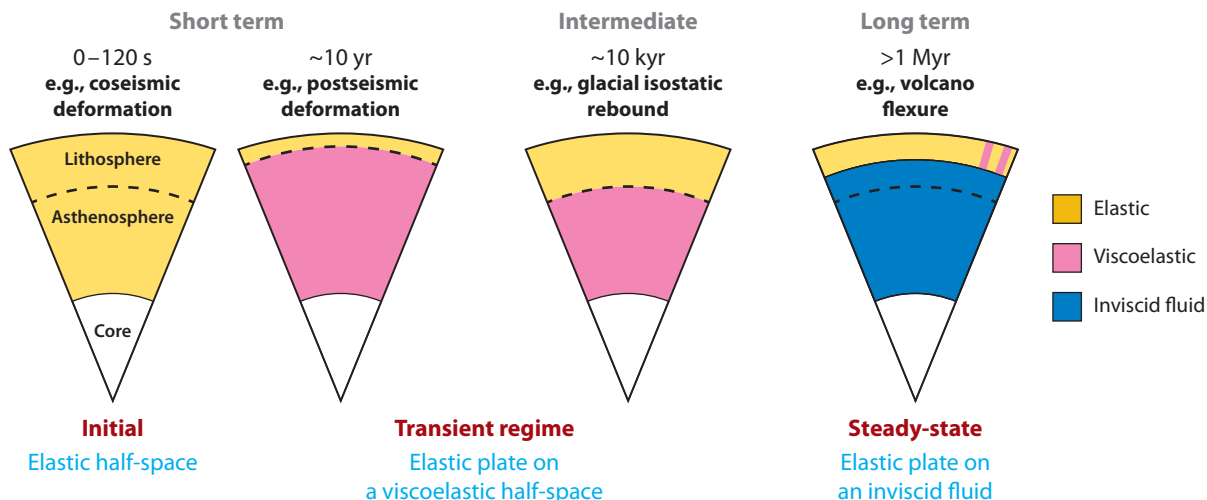


**Figure 1**

Schematization of the response of Earth's outermost layers to different types of load shifts on short-term, intermediate, and long-term timescales. Light blue text indicates the most commonly used rheological model at each timescale, and dark red text indicates the nature of the response.

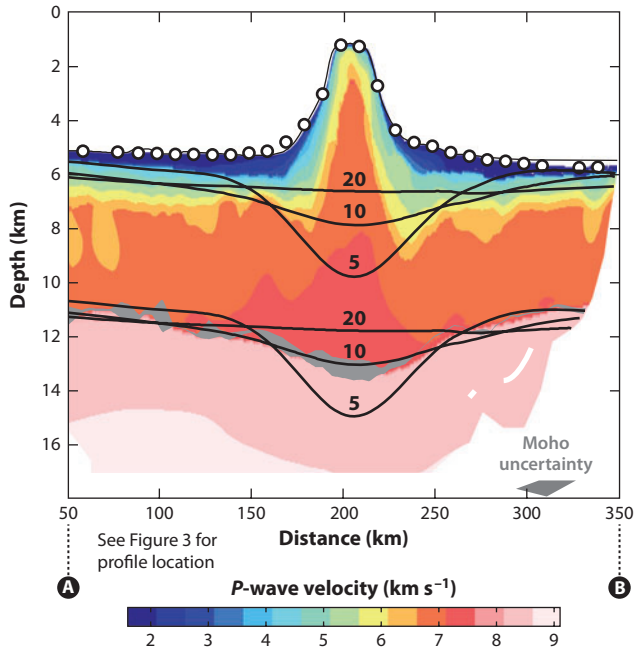


**Figure 2**

The crustal and upper-mantle structure along Profile AB, which intersects the crest of the Louisville Ridge seamount chain in the southwest Pacific Ocean at 27°35'S (Contreras-Reyes et al. 2010) (for profile location, see **Figure 3**). The colors indicate the  $P$ -wave velocity structure derived from a seismic refraction experiment involving a shooting ship (R/V *SONNE*) and ocean-bottom seismometers (*open symbols*). The solid black lines represent the predicted flexure of the crust and upper mantle assuming a load base at a depth of 4,910 m with densities of the infill, load, and mantle of 2,800, 2,800, and 3,400  $\text{kg m}^{-3}$ , respectively, and effective elastic thickness,  $T_e$ , of 5, 10, and 20 km. There is an excellent fit between the observed seismically constrained depth to Moho and the calculated depth based on the predictions of a simple elastic plate (flexure model) with  $T_e = 10$  km.

age. The purpose of this article is to use the results of oceanic and continental flexure studies in an attempt to derive a self-consistent model that describes how the lithosphere would behave for any load and plate age.

## 2. OCEANIC LITHOSPHERE

The oceans have had a simpler thermal and mechanical evolution and have undergone less significant erosion and sedimentation than have the continents and so show some of the best manifestations of flexure. The seafloor, for example, is littered with seamounts, most of which are volcanic in origin. Seamounts make ideal loads because they are concentrated (i.e., have a large edifice height to width ratio); formed rapidly ( $\sim 1\text{--}2$  Myr); and are usually emplaced on crust of known age, depth, and seismic structure. These factors allow the effects of flexure to be seen clearly, even on a volcano being carried along on a subducting oceanic plate moving into a deep-sea trench (**Figures 2** and **3**).

**Figure 4** shows a plot of the elastic thickness of the lithosphere,  $T_e$ , versus age for 98 estimates at seamounts and oceanic islands from each of the world's main ocean basins where the age of both the volcano and the underlying seafloor are known. The estimates are based on forward

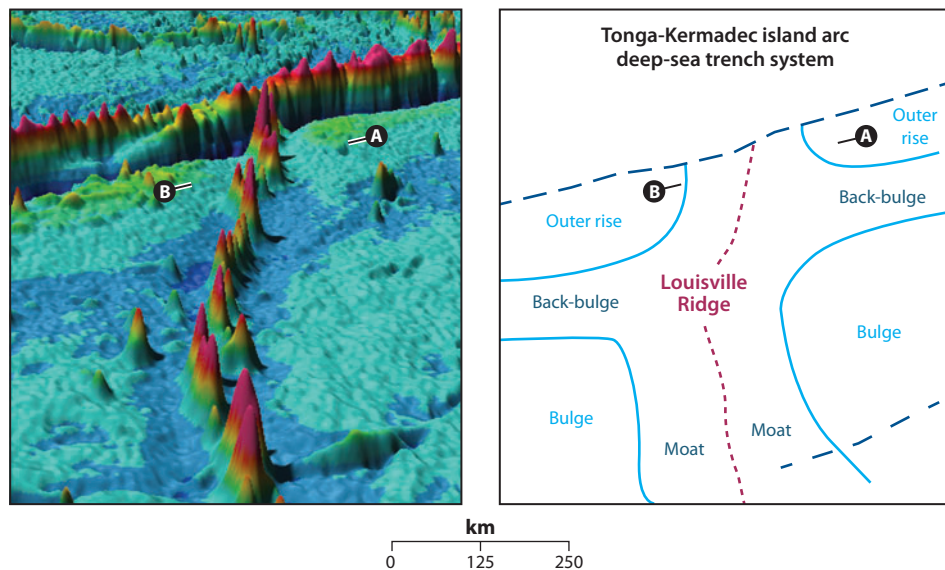


**Figure 3**

Perspective image (looking toward the northwest) of the free-air gravity anomaly along the Louisville Ridge seamount chain in the southwest Pacific Ocean. The gravity expression of the flexural bulge seaward of the Tonga-Kermadec trench, the flexural depression seaward of the trench as the “back-bulge”), and the flexural depressions that flank the Louisville Ridge are clearly visible in the figure. Note how the superposition of the gravity effect of the flexural depressions (*deep blue*) has produced a striking “cross” pattern in the free-air gravity anomaly. The image has been constructed from a high-pass filter of the satellite-derived free-air gravity anomaly grid of Sandwell & Smith (1997). The end coordinates of Profile AB (Figure 2) are indicated.

**Supplemental Material**

modeling (see data in **Supplemental Table 1**; follow the **Supplemental Materials link** from the Annual Reviews home page at <http://www.annualreviews.org>) where  $T_e$  is derived by a “trial and error” comparison of simple elastic plate model predictions to observations such as the gravity anomaly and bathymetry, seismically imaged surfaces of flexure, and vertical crustal motions. The model assumes linear elasticity and that any load or unload is supported partly by the flexural rigidity of the plate (a measure of its resistance to deformation) and partly by the buoyancy of the weak underlying foundation.  $T_e$  can be derived from the flexural rigidity, assuming the Young’s modulus,  $E$ , and Poisson’s ratio,  $\sigma$ . Laboratory measurements of  $E$  and  $\sigma$  have been carried out for oceanic and upper-mantle rocks to pressures of up to 1,000 MPa (Christensen 1978), but the values of these parameters on the long timescales of geological processes are not known. Most flexure studies assume  $E = 100$  GPa and  $\sigma = 0.25$ . Where other values have been assumed, we have corrected the  $T_e$  and shown the results in **Figure 4**. Error bars reflect uncertainties in the recovery of  $T_e$  and the age of the load and/or underlying seafloor where they have been quoted.

Despite the scatter, oceanic  $T_e$  generally increases with plate age and decreases with load age (**Figure 4a,b**). The scatter is smallest in **Figure 4c**, which shows a plot of  $T_e$  against the age of the plate *at the time of loading*. These data are well described by the depth to the 300–600°C oceanic isotherms based on a cooling plate model. Accordingly, as the plate increases its age away from a mid-ocean ridge, it increases in strength, and despite a possible decrease in  $T_e$  with load age, the plate retains a memory of this strength for long periods of time.

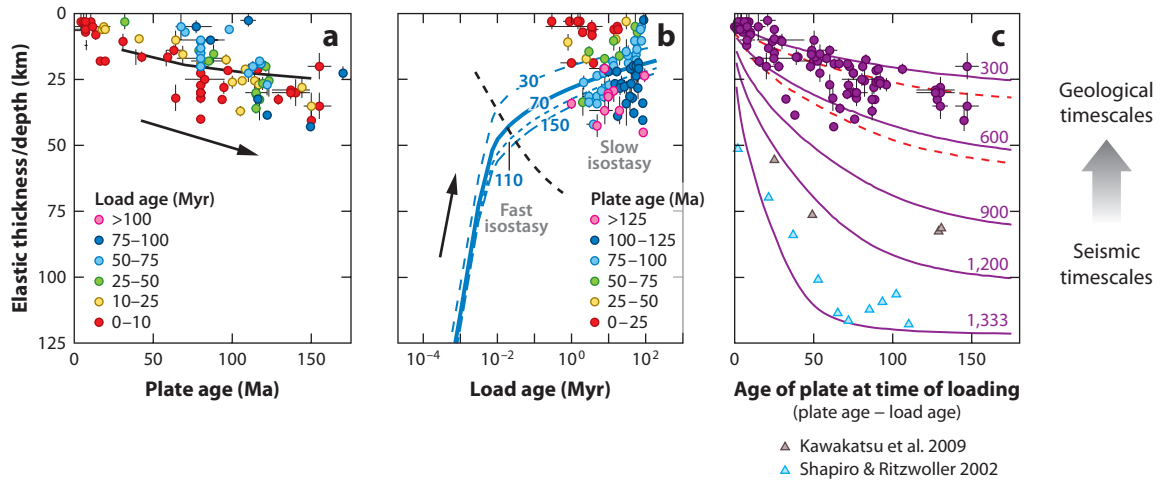


**Figure 4**

Plot of elastic thickness,  $T_e$ , versus age for seamounts and ocean islands, showing 98 total estimates. The estimates are based on table 6.1 in Watts (2001). Other estimates are from Freedman & Parsons (1986), Lyons et al. (2000), Collier & Watts (2001), Grevenmeyer et al. (2001), Zheng & Arkani-Hamed (2002), Minshull et al. (2003), Ali et al. (2003), Manea et al. (2005), Luis & Neves (2006), and Pim et al. (2008). See data in **Supplemental Table 1** for a complete list (follow the **Supplemental Materials link** from the Annual Reviews home page at <http://www.annualreviews.org>). (a)  $T_e$  versus plate age. The black line represents the predicted relationship between  $T_e$  and plate age for a multilayered viscoelastic plate model (Watts & Zhong 2000) with effective activation creep energy  $Q = 120 \text{ kJ mol}^{-1}$ , effective sublithospheric viscosity  $\eta_a = 10^{20} \text{ Pa s}$ , and a load age of 70 Ma. The model assumes a temperature structure for oceanic lithosphere given by the cooling plate model (Parsons & Sclater 1977) and that the decrease in viscosity from the cool, uppermost part of the oceanic lithosphere to the warm, lowermost part can be discretized into 17 individual viscoelastic layers. The arrow highlights a general increase of  $T_e$  with plate age. Colored symbols reflect load age. (b)  $T_e$  versus load age. Colored symbols reflect plate age. The blue lines represent the predicted relationship between  $T_e$  and load age for a multilayered viscoelastic plate model with  $Q = 120 \text{ kJ mol}^{-1}$ ;  $\eta_a = 10^{20} \text{ Pa s}$ ; and plate ages of 30, 70, 110, and 150 Ma. (c)  $T_e$  versus age of oceanic lithosphere at the time of loading. Purple circles represent the data plotted in panels a and b. Purple lines indicate the depth to the 300, 600, 900, 1,200, and 1,333°C oceanic isotherms based on a cooling plate model of Parsons & Sclater (1977). Red dashed lines indicate the depth to the 300 and 600°C isotherms based on the thermal model of McKenzie et al. (2005), which includes a dependency of the thermal conductivity on temperature. Triangles represent the seismic thickness of the lithosphere as determined using data from borehole broadband ocean-bottom seismometers (Kawakatsu et al. 2009) (*brown triangles*) and the depth to the 4.45  $\text{km s}^{-1}$  S-wave velocity, which defines the top of the low-velocity zone (Shapiro & Ritzwoller 2002) (*blue triangles*).

An important result (shown in **Figure 4c**) is that oceanic  $T_e$  is significantly less than the seismic thickness of the lithosphere, as defined by the depth to the top of the low-velocity zone (Shapiro & Ritzwoller 2002). In the continents, the depth to the top of the low-velocity zone corresponds closely to the depth to the top of the low-viscosity zone of glacial-isostatic studies. Because glacial-loading timescales are much shorter than those associated with volcano loading, the seismic thickness may be considered to be a short-term (i.e., a few seconds to a few tens of thousands of years) response to loading, in contrast to the elastic thickness, which is the response of the lithosphere to much longer geological timescales.

This distinction between the behavior of the lithosphere on short and long timescales has already been noted by Beaumont (1979), Anderson & Minster (1980), Watts et al. (1980), and Courtney & Beaumont (1983), among others. The lithosphere appears to respond to loading and unloading as a relatively thick structure at short timescales and a relatively thin one at long timescales. Watts & Zhong (2000) attributed the thinning to some sort of load-induced stress relaxation in the lithosphere, the consequence of which is to transfer stresses upward from the warm, less viscous, lowermost layer in the lithosphere to the cold, more viscous, uppermost layer,

which has a higher stress threshold than do the lower layers. The net result of this thinning is to weaken the lithosphere and cause the deformation to localize to the immediate vicinity of a load or unload.

The mechanism by which relaxation takes place in the lithosphere is not known, but experimental studies of subcrustal mantle rocks suggest that it involves some form of load-induced diffusion creep, dislocation creep, or low-temperature plasticity (e.g., Goetze & Evans, 1979, Karato & Wu 1993, Mei et al. 2010). The deformation can be described in simplified form by

$$\dot{\epsilon} = A\sigma^n e^{-Q/RT}, \quad (1)$$

where  $\dot{\epsilon}$ ,  $\sigma$ ,  $T$ , and  $R$  are the strain rate, stress, temperature, and gas constant, respectively;  $Q$  is the effective creep activation energy;  $n$  is the power-law exponent; and  $A$  is the pre-exponential constant that depends on pressure, grain size, and volatile content (e.g., Hirth & Kohlstedt 2003). The effective viscosity,  $\eta$ , at a particular temperature may be simplified as (e.g., Podolefsky et al. 2004)

$$\eta = \eta_a e^{\left[\frac{Q}{R}\left(\frac{1}{T} - \frac{1}{T_a}\right)\right]} \left[1 + \left(\frac{\sigma}{\sigma_T}\right)^{n-1}\right]^{-1}, \quad (2)$$

where  $\eta_a$  and  $T_a$  are the sublithospheric mantle viscosity and temperature, respectively,  $\sigma$  is the stress, and  $\sigma_T$  is the transition stress between dislocation and diffusion creep;  $n$  is equal to 1 for diffusion creep and  $\sim 3.5$  for dislocation creep. However, for low-temperature plasticity, the stress exponent  $n$  can be equal to 2, and the stress may also appear in the exponential function term (e.g., Mei et al. 2010).

The temperature structure of oceanic lithosphere can be estimated from bathymetry and surface heat flow data, and Equation (2) may be used to calculate the effective viscosity of the lithosphere as a function of depth for different values of the parameter pair,  $\eta_a$  and  $Q$ . Watts & Zhong (2000) used the cooling plate model of Parsons & Sclater (1977), a power-law exponent of  $n = 1$ , and a multilayered viscoelastic model to track the flexure and equivalent elastic thickness,  $T_e$ , as a function of age for an axisymmetric, seamount-type load emplaced on the surface of the oceanic lithosphere. They showed that the parameter pair that best fit the  $T_e$  data was  $Q = 120 \text{ kJ mol}^{-1}$  and  $\eta_a = 10^{20} \text{ Pa s}$ . A lower  $Q$  would require a higher  $\eta_a$ , whereas a higher  $Q$  would require a lower  $\eta_a$ . Regional variations in  $\eta_a$  and  $Q$  may therefore explain some of the scatter observed in  $T_e$  data.

Unfortunately, the observational evidence for a load-induced stress relaxation in oceanic lithosphere is limited. Many stratigraphic sequences, which might otherwise have recorded the response, such as those in the flexural moats that flank volcano loads, are incomplete owing to nondeposition, corrosive bottom countercurrents, or large-scale slope failures and mass wasting. However, the rapidity with which oceanic islands in French Polynesia, the Society Islands, and the Caroline Islands initially build up on the seafloor, become islands, and then subside (Watts & Zhong 2000); the long-term subsidence and uplift history of Ascension Island (Minshull et al. 2010); and the stratigraphic patterns of onlap and offlap in the moats flanking the Hawaiian Islands (Rees et al. 1993) and the Canary Islands (Collier & Watts 2001) all provide evidence indicating that some form of load-induced stress relaxation has, indeed, taken place in the oceanic lithosphere.

### 3. CONTINENTAL LITHOSPHERE

Compared with the oceans, continents have been subject to a wider range of load age (from a few seconds to several hundred tens of millions of years) and so have the potential to yield the best evidence for a lithosphere relaxation. The difficulty is that they have also had a more complex

thermal and mechanical evolution. Dominating their evolution, for example, is the Wilson cycle, which provides examples of structural inheritance; instances where rifted margins morph into mountain belts (and vice versa); and scenarios where a new landscape, once formed, is resurfaced by erosional or glacial processes. The Wilson cycle, therefore, adds complexity and makes it difficult to isolate the loads and the deformation that results from these loads in the continents.

The best examples of continental flexure may be the foreland basins that develop in front of a migrating fold and thrust loads at compressional plate boundaries (e.g., Beaumont 1981, Jordan 1981). Examples of such basins are found in the Himalayas (Ganges, Eurasia/Indo-Australia), the Alps (Swiss Molasse, Africa/Eurasia), and the Andes (Chaco Plain, Nazca/South America). Fold and thrust loads produce flexures that can be relatively easily identified by gravity anomaly as well as seismic and topography data. By comparing these flexures to the predictions of elastic plate models, we have learned a considerable amount about continental  $T_e$  and its relationship to age. Early studies (e.g., Karner et al. 1983, Willett et al. 1985) suggested, for example, that continental  $T_e$ , like oceanic  $T_e$ , is given by the depth to a particular isotherm. More recent studies (e.g., Watts 2001), however, have pointed out difficulties with this result, and no simple relationship has yet been established that links continental  $T_e$  with load and plate age.

Compounding the problem have been difficulties with the methods used to recover  $T_e$  in foreland basin settings. Among the difficulties are questions concerning the ratio of surface to subsurface loads, the continuity of the flexure surfaces, the position of any plate break, and the role that other factors such as erosional unloading (Burbank 1992) and dynamic topography (Liu et al. 2008) might play in controlling the large-scale “architecture” of foreland basins. Central to the debate has been the Ganges basin: Most researchers agree it developed, at least in part, during the Cenozoic by lithospheric flexure in front of thrust and fold loads in the Lesser and Greater Himalayas.

The Bouguer gravity anomaly and depth to basement over the central part of the Ganges basin have been compared with the predictions of a simple model in which the surface load of the Himalaya has been emplaced on a semi-infinite (i.e., broken) elastic plate with  $T_e = 40.0$  and 87.5 km (see **Figure 5**). Comparisons of observed and predicted Bouguer gravity anomaly and depth to the base of the foreland sequence provide support for the earlier conclusions of Lyon-Caen & Molnar (1983) and Karner & Watts (1983) showing that  $T_e$  of the subducting Indo-Australian plate must be high. The comparisons also show that a low  $T_e$  cannot explain the amplitude and wavelength of the observed data. Sensitivity tests show that changes in the load, infill, and mantle density within plausible limits (i.e.,  $\pm 100 \text{ kg m}^{-3}$ ) have little effect on these conclusions. The flexure model in **Figure 5** assumes a plate break that is located 285 km north of the Main Boundary thrust (MBT). This is possible because the plate break coincides with the Indus-Tsangpo suture, which marks the boundary between the converging Indo-Australia and Eurasia plates (e.g., Catlos et al. 2001). Sensitivity tests show that moving the plate break 100 km further north or south has only a small effect on the predicted Bouguer gravity anomaly and flexure and, hence, the recovered  $T_e$ . The main discrepancies are in the Bouguer anomaly over the Bundelkhand craton and the Lesser and Greater Himalayas, which we attribute to shallow geological structure and inaccuracies in the computation of the Bouguer correction, respectively.

Forward-modeling results, such as those shown in **Figure 5**, have been criticized by Jackson et al. (2008), among others, on the basis that they assume a priori the load and the location of the plate break. Therefore, we repeated the analysis using an inverse approach in which  $T_e$  is estimated directly from the Bouguer gravity anomaly using either a shape-fitting method (McKenzie & Fairhead 1997), which does not require a load to be specified, or a load method (e.g., Karner & Watts 1983) in which the load is prescribed by the present-day surface topography. Both methods assume a broken elastic plate model. The main difference between them is that the shape-fitting

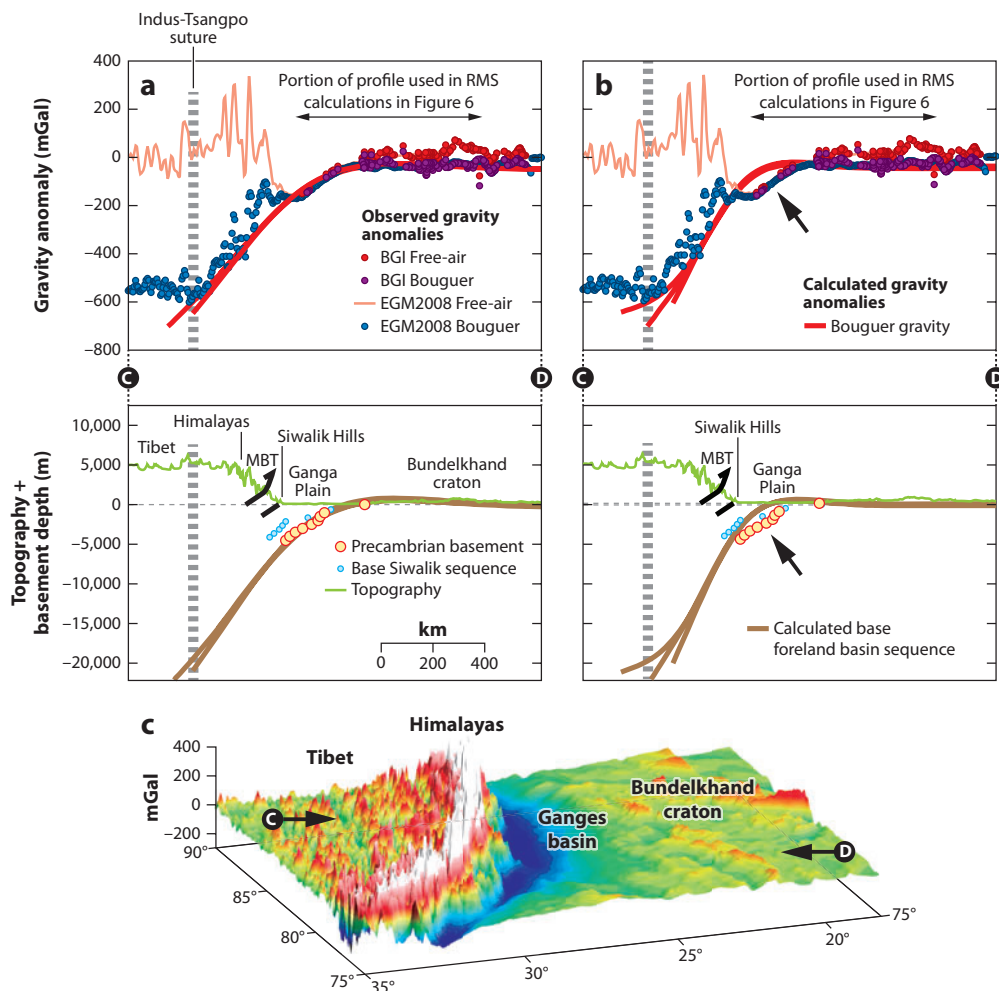


**Figure 5**

Comparison of the observed and calculated Bouguer anomalies and depth to the base of the foreland basin sequence along Profile CD of northern India, the Ganges basin, the Himalayas, and Tibet. The profile intersects the Main Boundary thrust (MBT), which separates the subducting Indo-Australian plate from the overthrusting Eurasian plate, at longitude 82.4°E and latitude 28.3°N. The observed gravity anomalies are based on “point” measurements compiled by the Bureau Gravimétrique International (BGI) (red and purple circles) and the 2.5' × 2.5' EGM2008 combined terrestrial and satellite derived free-air gravity anomaly grid of Pavlis et al. (2008) (thin red line). The EGM2008 field has been converted to Bouguer gravity anomalies (blue circles) using a fast Fourier transform method of calculating the gravity effect of the topography up to degree and order 4 (Parker 1972), a GEBCO topographic grid, and an average crustal density of 2,650 kg m<sup>-3</sup>. The calculated Bouguer gravity anomalies (thick red lines) and depth to the base of the foreland basin sequence (thick brown lines) are based on an elastic plate model with a load and infill density of 2,650 kg m<sup>-3</sup>, an effective elastic thickness,  $T_e$ , of 40.0 and 87.5 km and a plate break at a distance of 185, 285, and 385 km north of the MBT. The calculated Bouguer gravity anomaly has been referenced to the general level of the observed anomalies over the unflexed parts of the Bundelkhand craton, and the calculated depth to the base of the foreland basin sequence has been referenced to mean sea level. The Indus-Tsangpo suture (thick gray dashed line) is located 285 km north of the MBT. (a)  $T_e = 87.5$  km. (b)  $T_e = 40.0$  km. Thick black arrows highlight the region of the largest discrepancy between the observed and calculated Bouguer gravity anomalies and depth to the Precambrian basement. Thin black horizontal arrows delineate the portion of Profile CD used in the no-load method, the northern edge of which is defined by the first hint of load and/or upward inflection in the Bouguer gravity anomaly that appears nonflexural. The profile used in the load method is extended into Tibet at the same azimuth. (c) Perspective view (from the northwest) of the EGM2008 free-air gravity anomaly field over the Himalayas and Ganges basin and the outer rise of central India. Arrows show the location of Profile CD in panels a and b.

method makes no assumptions about the loads acting on the plate and solves for a vertical shear force and bending moment that act at the load edge, whereas the load method assumes the shape of the load and solves for the position of the plate break beneath the load.

**Figure 6** shows that the shape-fitting and load methods yield quite different values of  $T_e$ . The minimum of the root mean square (RMS) difference between the observed and calculated Bouguer anomaly for the shape-fitting method is for  $T_e = 18.0$  km, whereas the minimum for the load method is for  $T_e = 81.0$  km. The RMS minimum is lower in the shape-fitting method (8.4 mGal) than in the load method (10.7 mGal), and the fit between observed and calculated Bouguer gravity anomaly over the foreland basin is better.

Problems with the application of the shape-fitting method to the central Ganges basin are that the bending moment of  $-7.9 \times 10^{16}$  N m and the vertical shear force of  $2.0 \times 10^{12}$  N required to fit the Bouguer gravity anomaly and flexure are difficult to interpret geologically. This is because synthetic tests show that a negative bending moment in the immediate vicinity of the load flank is unlikely. We have loaded a broken elastic plate, for example, with a distributed surface load and then applied different combinations of positive and negative bending moments and vertical shear forces at the plate break and found that only positive bending moments are generated at the load edge. Interestingly, when we use the shape-fitting method, together with a constraint that the applied bending moment is positive, then we obtain high  $T_e$  values, similar to those derived earlier using the load method (e.g., Karner & Watts 1983, Lyon-Caen & Molnar 1983).

Because of this difficulty, we believe that using the actual fold and thrust loads responsible for the flexure is preferable when modeling the flexure of subducting continental plates. The position and size of these loads can often be recovered from structural restorations and balanced geological cross sections. Alternately, the present-day topography may be used because we know that it comprises at least part of a cumulative stack of individual fold and thrust loads.

The only outstanding questions pertain to the sensitivity of  $T_e$  to the plate break position and the relative proportion of surface (i.e., topographic) to subsurface (i.e., buried) loads. We found (**Figure 6b**), however, that the position of the plate break beneath the topographic load has little effect on the  $T_e$  that is recovered, in accord with the results in **Figure 5**. Flexure studies in Taiwan (Lin & Watts 2002) and Oman (Ali & Watts 2009) showed that subsurface loads are distinguished by their large-amplitude, short-wavelength, Bouguer and isostatic (Airy) gravity anomaly highs and flanking lows. The absence of such anomalies in the Himalayas suggests that surface loads dominate here over subsurface loading. Thus, if we assume a plate break at the Indus-Tsangpo suture and that the only loads acting on the subducting plate are surface loads, then our results confirm that  $T_e$  of the Bundelkhand craton in northern India is high. Only a high value that exceeds the local crustal thickness is capable of explaining *both* the width and depth of the Ganges foreland basin.

The possibility that  $T_e$  of cratons is high is supported by spectral admittance and coherence studies from other continents. These methods, which are based on an analysis of the relationship between gravity and topography as a function of wavelength, repeatedly recover high  $T_e$  in cratonic North America (Wang & Mareschal 1999, Fluck et al. 2003), South America (Ussami et al. 1993, Tassara et al. 2006), Europe (Pérez-Gussinyé & Watts 2005), Africa (Hartley 1995, Pérez-Gussinyé et al. 2009), and Australia (Swain & Kirby 2006). There are exceptions and not all cratons have a uniformly high  $T_e$ . For example, the central Indian shield appears to be characterized by both high and low values (Tiwara & Mishra 1999, Jordan & Watts 2005).

However, difficulties also arise with the spectral methods. The window size, for example, needs to be large enough to resolve a high  $T_e$ , if it is present, but small enough to avoid “smearing” across different geological features (Kalnins & Watts 2009). Other difficulties concern the low coherence that is usually observed between the free-air gravity anomaly and topography over cratons, the type of taper to apply to the edges of these data, and the wide range of methods used to obtain smooth

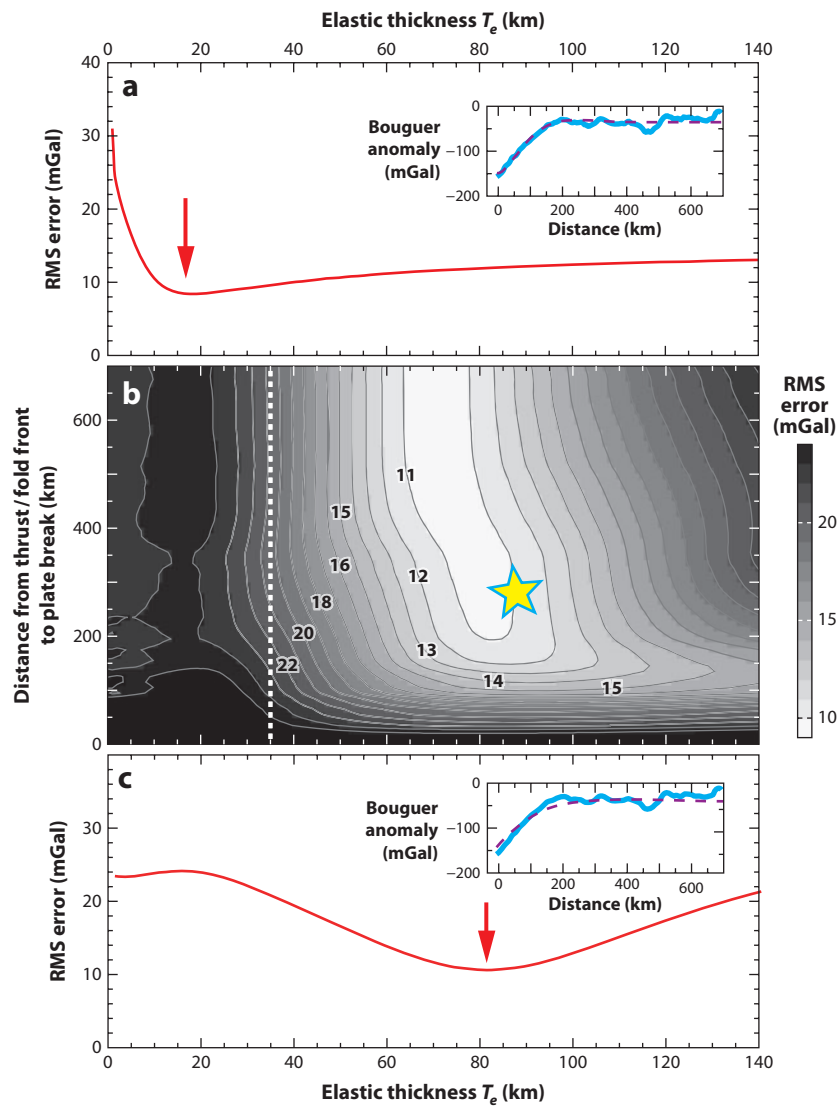


**Figure 6**

Comparison of observed Bouguer gravity anomalies along a portion of Profile CD south of the Main Boundary thrust (MBT) (as delineated by the horizontal arrows in the upper panels of **Figure 5**) to calculated anomalies based on two different methods of loading a semi-infinite (i.e., broken) elastic plate. (a) Shape-fitting method of McKenzie & Fairhead (1997). Red line shows the root mean square (RMS) error between observed and calculated Bouguer gravity anomalies  $0 < T_e < 140$  km. (Inset) Comparison of the observed (solid light blue line) and calculated Bouguer gravity anomaly at the RMS minima (dashed purple line). (b) Load method (e.g., Karner & Watts 1983). Contours show the RMS error for a plate break 0–700 km north of the MBT and  $0 < T_e < 140$  km. Yellow star indicates the high  $T_e$  case modeled in **Figure 5b**. Thick dashed white line represents the estimated crustal thickness. (c) Load method. Red line and inset as in panel a.

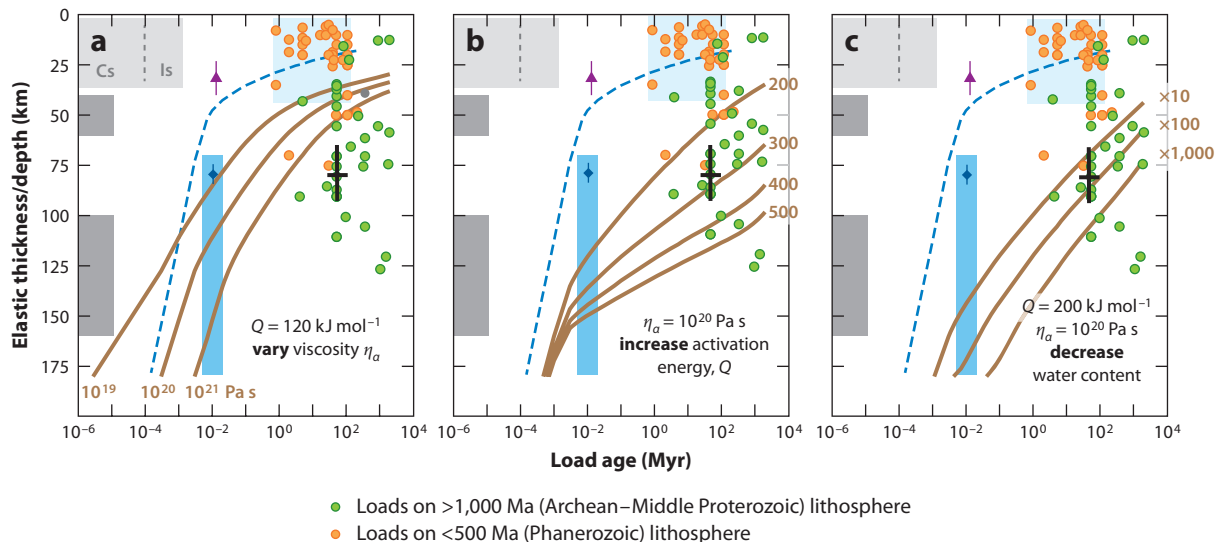


**Figure 7**

Plot of elastic thickness,  $T_e$ , versus load age for foreland basins and rim flank uplifts. Number of estimates = 86. See data in **Supplemental Table 2** (follow the **Supplemental Materials link** from the Annual Reviews home page at <http://www.annualreviews.org>) for a list. Orange and green circles represent loads on lithosphere with thermotectonic age <500 Ma and >1,000 Ma, respectively. Blue dashed lines indicate predictions based on a multilayered viscoelastic model with a 70 Ma oceanic geotherm (**Figure 8**) and different values of the effective activation energy,  $Q$ , and effective reference viscosity,  $\eta_a$ . (a) Constant  $Q$  ( $120 \text{ kJ mol}^{-1}$ ) and  $10^{19} < \eta_a < 10^{21} \text{ Pa s}$ . (b) Constant  $\eta_a$  ( $10^{20} \text{ Pa s}$ ) and  $200 < Q < 500 \text{ kJ mol}^{-1}$ . (c) Constant  $Q$  and  $\eta_a$  and decrease in water content by a factor of 10, 100, and 1,000. Colors and symbols for panels a–c are as follows: range of oceanic  $T_e$  from **Figure 4** (light blue shaded region); short and intermediate timescale loads on the continents (other shaded regions); estimates derived from rebound following the last glacial maxima (e.g., Peltier et al. 2002, Zhong et al. 2003, Latychev et al. 2005) (blue shaded region); InSAR- and GPS-determined fault bottom depth and centroid depths of earthquakes that are summarized in tables 1–4 of Wright et al. (2013) (light gray shaded region); GPS-determined thickness of the Pacific and Indo-Australian plates in New Zealand (Cohen & Darby 2003) (dark gray shaded region); Lake Bonneville (Iwasaki & Matsu’ura 1982) (purple triangles); Richmond Gulf (Walcott 1973) (dark blue diamonds); the best fit values for the Ganges foreland basin along Profile CD (**Figures 5 and 6c**) (thick black crosses). Abbreviations: Cs, coseismic deformation; Is, interseismic deformation.

spectra. Sacke & Ussami (2009) compared multitaper fast Fourier transform (Pérez-Gussinyé et al. 2007), wavelet (Tassara et al. 2006), and forward-modeling (Stewart & Watts 1997) methods of analyzing gravity and topography data and showed that the best fit to the seismically constrained depth to basement in the central Andes foreland basin is for the  $T_e$  structure deduced from forward modeling.

**Figure 7** shows a plot of continental  $T_e$  versus load age based on only 69 forward-modeling (i.e., nonspectral) estimates at foreland basins and rim flank uplifts (see **Supplemental Table 2**). Individual estimates have been color coded according to the thermotectonic age of the basement. All estimates have been plotted so that in the modeled case of the Ganges foreland basin we included the older results of Karner & Watts (1983), Lyon-Caen & Molnar (1983), and Jordan & Watts (2005) as well as the more recent results of Jackson et al. (2008). The black cross in **Figure 7** shows the estimate (with approximate error bars) that was derived using the inverse load method in this article. For reasons of clarity, error bars for other estimates in the figure, which range in  $T_e$  and age up to  $\pm 10 \text{ km}$  and  $\pm 200 \text{ Ma}$ , respectively, have been omitted. We attribute the larger age uncertainty found in the continents than in the oceans to the difficulty of assigning a

Supplemental Material

thermotectonic age, for example, when an Archean craton has been reactivated during more than one episode of Phanerozoic deformation.

The main result shown in **Figure 7** is that, like the oceans, continents show a general dependence of  $T_c$  on plate age. Loads on young (<500 Ma, i.e., Phanerozoic) lithosphere generally have a lower  $T_c$  (mean = 23.7 km,  $N = 35$ ) than loads of similar age on old (>1,000 Ma, i.e., Archean–middle Proterozoic) lithosphere (mean = 65.1 km,  $N = 34$ ). The mean of all the continental  $T_c$  estimates is 43.9 km, and the RMS deviation is 30.6 km ( $N = 86$ ), which is significantly smaller than the 90–110 km depth to the lithosphere/asthenosphere boundary derived from converted seismic phases (Rychert et al. 2005), the 80–220 km seismic thickness derived from controlled source and teleseismic body wave phases (e.g., Gaherty et al. 1999), and the 150–280 km thermal thickness of the lithosphere (Priestley & McKenzie 2006) derived from shear wave velocities and geothermal gradients. They are also generally less than the 90–120 km elastic “lid” thickness commonly assumed in glacial isostatic studies (e.g., Peltier et al. 2002). Therefore, similar to the oceans, the continents appear to show a relationship between the short-term seismic thickness and long-term elastic thickness.

An interesting question then is whether the same multilayered viscoelastic model that accounts for oceanic  $T_c$  can explain the continental  $T_c$  estimates. Accordingly, to match model deformations to those of a simple elastic plate model, we used the multilayered viscoelastic model of Watts & Zhong (2000), together with a temperature structure to define the viscosity, and tracked the equivalent elastic thickness at different ages since loading. As in Watts & Zhong (2000), we initially assumed a power-law exponent of  $n = 1$ . However, we also considered cases where  $n > 1$ .

A potential problem with applying a multilayered viscoelastic model to the continents is prescribing the temperature structure. Unlike the oceans, there is no thermal model that describes the temperature structure of continental lithosphere as a function of age. We therefore followed McKenzie et al. (2005) and assumed a temperature structure based on pressure and temperature data derived from the Jericho kimberlite in the Slave Province, Canadian Shield. Such a temperature structure is consistent with surface heat flow data (Mareschal & Jaupart 2004) and is considered representative of cratonic regions. **Figure 8** shows the temperature and the corresponding viscosity structure, assuming an effective creep activation energy  $Q = 200 \text{ kJ mol}^{-1}$ , sublithospheric mantle viscosity  $\eta_a = 10^{20} \text{ Pa s}$ , and power law  $n = 1$ . As shown in **Figure 8**, the viscosity decreases by several orders of magnitude with depth, which compares well to the calculations for cratons of Dixon et al. (2004), who took into account grain size, fugacity, and water content.

In **Figure 7**, the continental  $T_c$  estimates are compared with calculations based on the multilayered viscoelastic model with the Jericho kimberlite temperature profile,  $n = 1$ , and different values of the  $\eta_a$  and  $Q$  parameter pair. **Figure 7a** shows that a model in which  $Q = 120 \text{ kJ mol}^{-1}$  (i.e., the same value that explains the oceanic  $T_c$  data) and  $\eta_a$  is varied cannot explain the full range of the continental  $T_c$  data. This is because the computed curves converge as load age increases owing to the presence of a strong uppermost layer of the lithosphere, which behaves essentially as an elastic plate at long timescales, irrespective of the value of  $\eta_a$ . A better fit (**Figure 7b**) is obtained, however, if  $\eta_a$  is fixed and  $Q$  is varied. For example,  $\eta_a = 10^{20} \text{ Pa s}$  and  $200 < Q < 500 \text{ kJ mol}^{-1}$  generally explain the spread of the continental  $T_c$  data. The main discrepancies are for foreland basins formed on young (<0.5 Ga) continental lithosphere, which imply much lower values. These estimates include, for example, the Transverse Ranges, California, (Sheffels & McNutt 1986) and the west Taiwan basin (Lin & Watts 2002) where the geotherm is likely to be more elevated than the one assumed here.

A situation in which the subcrustal continental mantle has a higher effective activation energy than the subcrustal oceanic mantle is potentially problematic, however, given that their

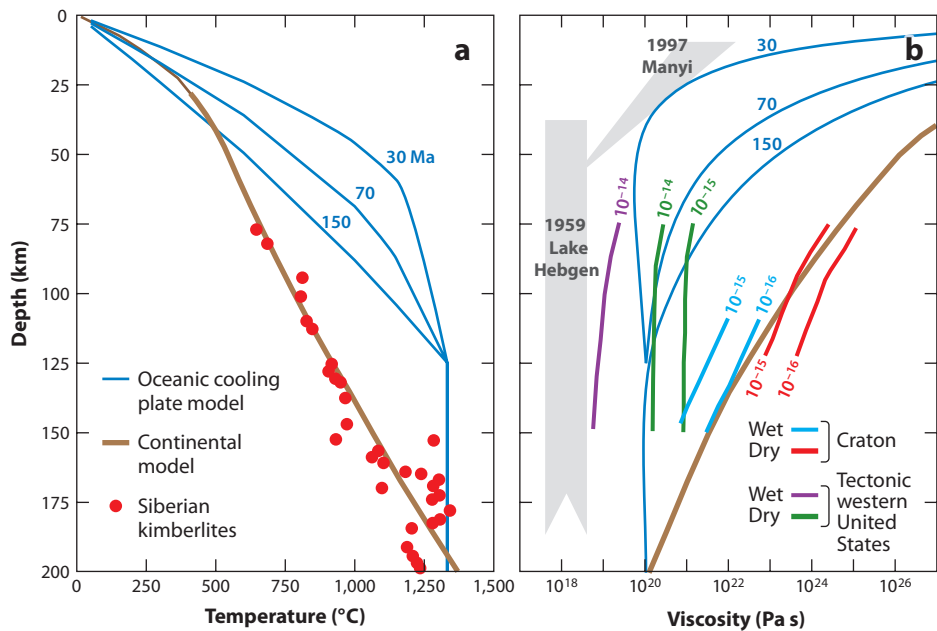


**Figure 8**

Plots of temperature and viscosity as a function of depth for continental lithosphere. (a) Temperature versus depth: the temperature versus depth profile that best fits pressure and temperature estimates from nodules from the Jericho kimberlite in northern Canada (McKenzie et al. 2005) (*thick brown curve*); the temperature versus depth profiles for 30, 70, and 150 Ma oceanic lithosphere based on the cooling plate model of Parsons & Sclater (1977) (*dark blue lines*). (b) Viscosity versus depth. The viscosity has been computed from the temperature structures in panel a: the viscosity calculated by Dixon et al. (2004) for “dry” (*red*) and “wet” (*light blue*) rheologies in cratons and dry (*green*) and wet (*brown*) rheologies in the tectonic western United States for “geological” strain rates in the range of  $10^{-16}$  to  $10^{-14}$   $s^{-1}$  (*short solid colored lines*); the InSAR- and GPS-determined viscosity structure associated with the deformation that followed the western US 1959 Lake Hebgen (Nishimura & Thatcher 2003) and the southern Tibet 1997 Manyi (Yamasaki & Houseman 2012) earthquakes (*light gray shaded regions*).

composition, body wave velocity, and isotope geochemistry are essentially the same (e.g., Allègre et al. 1981). Another possibility, therefore, is that oceanic and continental activation energies are both relatively low, but the strength of the subcrustal continental mantle is enhanced by dehydration. We constructed a model, shown in **Figure 7c**, where  $\eta_a$  and  $Q$  are as deduced by Watts & Zhong (2000) for oceanic lithosphere, but the degree of dehydration of the subcrustal continental mantle is varied by a factor of 10 to 1,000. We know, for example, that arc volcanism is caused by subducting slab-related dehydration and partial melting at depth (e.g., Hirth & Kohlstedt 2003). Seismic tomography and plate reconstructions also demonstrate that subducting slabs have a propensity to accumulate beneath cratonic lithosphere in the geological past (e.g., Humphreys et al. 2003). Other evidence for dehydration of the subcontinental mantle has come from considerations of the long-term stabilization of the continents (Houseman & Molnar 2001). **Figure 7c** shows that a dehydrated continental mantle, together with a low  $Q$ , can help explain the spread of continental  $T_c$  data, particularly the high values on old (>1,000 Ma) cratonic lithosphere.

An alternative possibility that removes the requirement for dehydration is that the subcrustal continental and oceanic mantle lithosphere both have relatively high activation energies but are characterized by different creep mechanisms. If the continental subcrustal mantle deforms by

diffusion creep ( $n = 1$ ), then (as shown in **Figure 7**)  $\eta_a = 10^{20}$  Pa s and  $200 < Q < 500$  kJ mol<sup>-1</sup> fit the data well. By contrast, if the oceanic subcrustal mantle deforms by dislocation creep ( $n = 3.5$ ), then relatively high activation energies may also account for the oceanic  $T_e$  data. This is because increasing  $Q$  strengthens the lithosphere, but increasing  $n$  weakens it. Support for the possibility of dislocation creep in the oceanic subcrustal mantle has come from Asaadi et al. (2011), who argued that the downstream decay of swell topography generated by the Hawaiian plume requires dislocation rather than diffusion creep, and van Hunen et al. (2005), who argued that the seismic structure of Pacific lithosphere requires that sublithospheric small-scale convection operates in the dislocation creep rather than the diffusion creep regime. Therefore, these considerations suggest that the long-term behavior of oceanic and continental lithosphere may be controlled, at least in part, by regional differences in the creep mechanism in the subcrustal mantle.

Irrespective of the relative role of water and regional variations in the creep mechanism on mantle rheology, it is clear from **Figure 7** that a model in which  $\eta_a = 10^{20}$  Pa s and a cratonic geotherm cannot account for the short-term geodetic- and seismogenic-determined estimates of elastic plate thickness (e.g., Wright et al. 2013). This is despite evidence from postseismic deformation for the occurrence of some form of viscoelastic relaxation in the lower crust and mantle (e.g., Pollitz 2003, Vergnolle et al. 2003). GPS studies of the deformation associated with individual earthquakes [e.g., 1959 Lake Hebgen earthquake (Nishimura & Thatcher 2003), 1997 Manyi earthquake (Yamasaki & Houseman 2012)], however, suggest viscosities for the lower crust and mantle ranging from  $3 \times 10^{16}$  to  $4 \times 10^{18}$  Pa s (**Figure 8**), which are significantly lower than those used to model the  $T_e$  estimates in **Figure 7**. Furthermore, geodetic and seismogenic data are mainly confined to regions of active deformation (e.g., basin and range, Southern Tibet) where there is evidence of elevated temperatures (Saltus & Thompson 1995, Chan et al. 2009). We expect from extrapolation of the calculated curves in **Figure 7** that a multilayered viscoelastic model with a low sublithospheric mantle viscosity and an elevated geotherm would account for at least some of the geodetic- and seismogenic-determined elastic thickness data. Therefore, the phenomenon of viscoelastic relaxation, together with regional variations in geotherm, provides a remarkably simple first-order model for lithosphere behavior that appears to be applicable across a wide range of timescales.

#### 4. DISCUSSION

As discussed above, irrespective of the lithosphere's actual rheological structure,  $T_e$  data in the oceans and continents are consistent with a model in which the subcrustal mantle lithosphere undergoes some form of relaxation when loaded or unloaded. Using a symmetric, >1-Myr-old volcano load with a height of 4 km and a base radius of 40 km and a top radius of 20 km that is emplaced on 70 Ma oceanic lithosphere, Watts & Zhong (2000) showed that the subsidence follows a simple exponential decay with a relaxation time (i.e., the time needed for the subsidence to reach  $1/e$  of its final value) of  $\sim 5 \times 10^4$  yr. The relaxation is initially rapid but slows significantly as stress relaxation shifts from the deep, warm, and less viscous layer of the lithosphere to the shallow, cold, and more viscous layer, making it behave on long timescales essentially similar to an elastic plate.

The model calculations in **Figure 7** show that the subcrustal continental mantle lithosphere has a wider "dynamic range" of possible viscosity and, hence, equivalent elastic layer thickness versus depth profiles than does oceanic lithosphere; thus, the former is expected to show a greater range of possible relaxation times, with some lower than  $\sim 5 \times 10^4$  yr and some higher, depending on tectonic setting. The combined flexure, glacial isostatic rebound and geodetic- and seismogenic-determined elastic thickness data plotted in **Figure 7** suggest relaxation times in the range of a

few days to billions of years. The shortest are the relaxation times ranging from  $10^{-1}$  to  $10^1$  yr, deduced for the lower crust and mantle from geodetic and seismogenic data. The longest are associated with the flexure of  $>1,000$  Ma continental lithosphere. The relaxation times deduced from glacial isostatic rebound studies (Walcott 1973, Peltier 2002) are intermediate and in the range  $3 \times 10^3$  to  $1 \times 10^4$  yr, but they refer to the sublithospheric rather than the lithospheric mantle. Nevertheless, per the data shown in **Figure 7**, lithosphere relaxation is pervasive and will have significance that extends beyond flexure to isostatic studies in general. Therefore, we further examine some of these studies here.

#### 4.1. Sedimentary Basin Formation

We know from backstripping (e.g., Watts & Ryan 1976) that sediment and water loading and unloading are major contributors to the stratigraphic “architecture” of sedimentary basins, affecting their patterns of onlap and offlap and, in some cases, their facies. Most stratigraphic models that combine the effects of sediment and water loading and unloading with tectonic subsidence and uplift (e.g., due to thermal contraction and uplift), however, are based on idealized elastic plate models. Although these models often consider the effect of an elastic thickness that varies, for example, with age since a rifting event, they generally ignore any dependency on the elastic thickness with load age.

Notable exceptions include the work of Sleep & Snell (1976), Sweeney (1977), Beaumont (1978), and Quinlan & Beaumont (1984) and their coworkers during the late 1970s and early 1980s. These workers showed that a model of a viscoelastic plate overlying an inviscid fluid substrate could explain the large-scale stratigraphic “architecture” of the East Coast, United States, rifted continental margin; the Alberta and Allegheny foreland basins; and the Michigan and Sverdrup cratonic basins. These basins are dominated by offlap at their edges, and a uniform viscoelastic plate with a relaxation time of  $\sim 50$  Myr predicts a gradual narrowing and deepening of the basin through time and offlap at its edges. However, as Sloss & Scherer (1975) showed, sedimentary basins generally widen rather than narrow with time and are dominated by onlap, not offlap, at their edges. The architecture of these basins can be explained by an elastic plate model, which predicts onlap following heating at the time of rifting, as the lithosphere cools, and orogenic loading, as the basin fills. Such a model is also in accord with offlap at the edge of a basin, if the basin was subsequently subject to a regional erosional event due to either tectonic uplift or a sea-level fall.

**Figure 9** shows the stratigraphy that would be expected for a basin that develops on a multi-layered viscoelastic continental plate. We assume a model in which the accommodation space has been created by an axisymmetric, downward-acting load and the sediments completely infill the flexure for each time increment, except the most recent one. Because basins develop in a range of tectonic settings, we have considered two creep mechanism models: diffusion creep ( $n = 1$ ) and dislocation creep ( $n = 3.5$ ). The diffusion creep model is based on the analytical method described in Zhong (1997) and Watts & Zhong (2000), whereas the dislocation creep model utilizes the finite element modeling method of Zhong et al. (2003). Both models invoke the same temperature structure and show similar stratigraphic patterns with an initial phase of onlap followed by offlap and a short relaxation time, when viscous strains exceed elastic ones. The main difference is that the deformation is more localized within the dislocation creep than within the diffusion creep.

The downward-acting load used to model the stratigraphy in **Figure 9** could have resulted from tectonic processes associated with either an extensional or a compressional event. Irrespective of the actual load source, the effects of lithosphere relaxation are to increase the

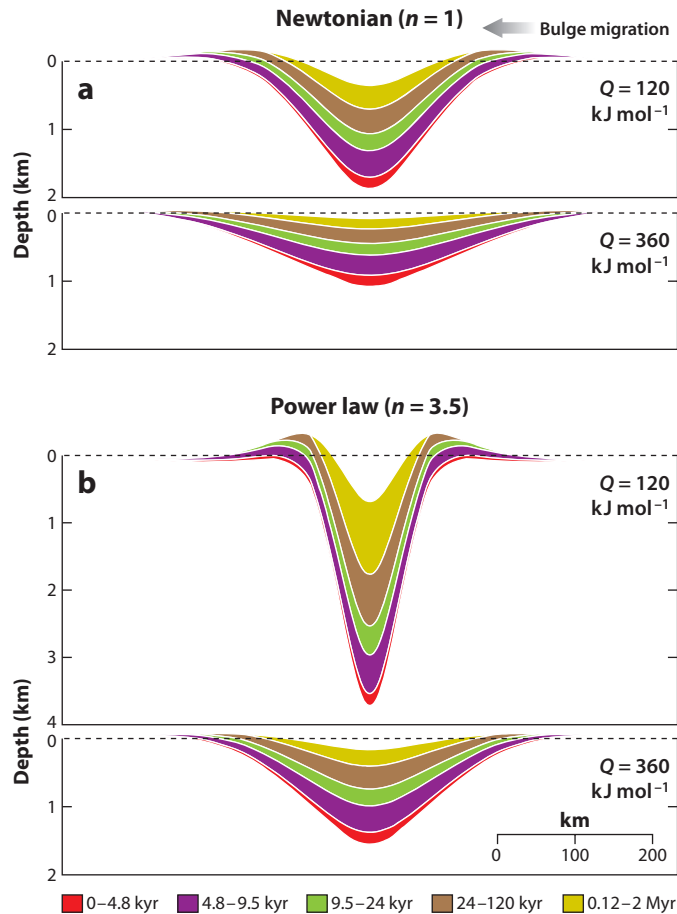


**Figure 9**

A two-dimensional, finite element, multilayered viscoelastic model for the evolution of a sedimentary basin. The model is based on Zhong et al. (2003) and assumes a box measuring 600 km deep and 3,000 km wide, with a load that is 5 km high, 80 km wide at the base, and 60 km wide at the top. The shear modulus was assumed to be  $3.33 \times 10^{10}$  Pa. The viscosity was derived from the temperature structure of 80 Ma oceanic lithosphere, a sublithosphere mantle viscosity of  $10^{20}$  Pa s, and a rheology with power-law exponent with either (a)  $n = 1$  (i.e., Newtonian) and effective creep activation energy  $Q = 120 \text{ kJ mol}^{-1}$  and  $Q = 360 \text{ kJ mol}^{-1}$  or (b)  $n = 3.5$  (i.e., non-Newtonian) and  $Q = 120 \text{ kJ mol}^{-1}$  and  $Q = 360 \text{ kJ mol}^{-1}$ . As shown, all four rheological models predict stratigraphic onlap followed by offlap, as viscous effects become more dominant than elastic ones. Also,  $n = 3.5$  localizes the deformation closer to the region of loading than occurs in the  $n = 1$  case. Increasing  $Q$  broadens the basin and shallows it in both cases.

accommodation space and then decrease it such that any sediment that accumulates changes in grain size upward from fine at the bottom to coarse at the top. Repetitive events could generate cyclothem. Lithologic cycles of limestone, marl, and shale, for example, are commonly observed in the geological record where they are often attributed to Milankovitch orbital-induced climatic variations. **Figure 9** shows, however, that lithosphere relaxation following loading and unloading may contribute to some of these cycles—even to ones of relatively short duration (i.e., 1–2 Myr).

## 4.2. Sea-Level Change

Much discussion has recently focused on sea-level change, its link to global warming, and its impact on the position of shorelines. Sea-level rise and fall will flexurally load and unload a shelf edge, so examining the influence that lithosphere relaxation may have on the shape of an ocean margin is useful, especially as it impacts the fluvial profile and the flux of sediment into a basin.

As Bloom (1967) first showed, the position of a shoreline on a shelf subject to sea-level change depends on how it adjusts isostatically to water loading and unloading. Consider, for example, a sea-level rise,  $b$ , that should cut a notch, once equilibrium is reached. The additional water, however, acts as a load that will depress the shelf, together with the adjacent deep ocean floor. Precisely where on the shelf a notch is cut depends, however, on the relative rate of the sea-level rise and the isostatic adjustment. If the rate of isostatic adjustment is slow compared with the rate of sea-level rise, then a notch will initially be cut relatively high up on a shelf. Then, as the margin adjusts and sinks under the water load, another notch will be cut lower down on the shelf. If the rate of isostatic adjustment is fast, then a notch will not be cut high up on the shelf and the shoreline will proceed directly to cutting the lower notch. The implication for the magnitude of sea-level change is that the vertical height between the uppermost and lowermost notches will directly reflect  $b$  in the slow case, whereas it will reflect  $(b - y)$  in the fast case, where  $y = b^* \rho_w / \rho_m$  and  $\rho_w$  and  $\rho_m$  are the densities of water and mantle, respectively, assuming Airy isostasy.

If the ocean floor and shelf are coupled, then it is important, as Chappell (1974) demonstrated, to take into account the flexural strength of an ocean margin when considering loading and unloading due to sea-level change. This was demonstrated by Hutton et al. (2013), who used an analytical expression for a triangular-shaped water load and unload to show that flexure would rotate the initial depositional slope and, hence, alter the fluvial profile and, potentially, the sediment flux into a basin. These authors did not consider, however, time-dependent flexure, such as would be associated with lithosphere relaxation.

**Figure 10** shows the time-dependent flexure that would be expected following a sea-level rise of 100 m on a shelf with a grade of 1:50,000, which is typical of many present-day continental shelves. In this case, the load is triangular in shape and asymmetric. Accordingly, we used the method of Brotchie & Silvester (1969), which is based on the correspondence principle, to calculate the flexure of a uniform viscosity plate overlying an inviscid fluid from its initial and final elastic thickness. The figure shows a broad initial flexure that extends seaward and landward of the shelf. Then, as time elapses, the shelf tilts such that the flexure seaward of the shelf increases while the flexure landward of the shelf decreases. The sea-level datum, however, remains fixed because the increase in accommodation space seaward of the shelf will be infilled by water that is displaced by the decrease in accommodation space landward of the shelf.

As predicted using the model in **Figure 10**, a sea-level rise will force the shoreline inland initially, but it will then move seaward as the lithosphere relaxes under the water load. A sea-level fall will have an opposite effect. The rate of shoreline migration depends on the viscosity structure of the lithosphere, which may vary spatially, depending, for example, on whether young Phanerozoic or old Archean and Proterozoic lithosphere (**Figure 7**) is involved in the water loading or unloading. The model of sea-level rise assumed here, which is based on a uniform viscosity of  $1.6 \times 10^{21}$  Pa s, implies a shoreline that has migrated seaward  $\sim 90$  km in  $\sim 2$  kyr. A lower viscosity lithosphere would result in a greater shoreline shift, whereas a higher viscosity lithosphere would result in a smaller shift in the same time. These shifts are significant because they show that a shoreline may not always migrate landward in response to sea-level rise or migrate seaward in

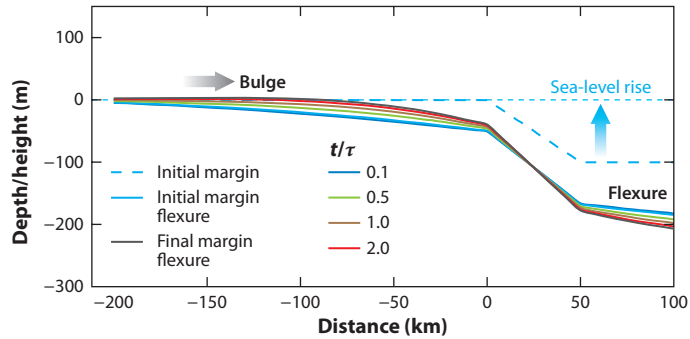


**Figure 10**

Simple viscoelastic plate model showing the flexure of a continental shelf in response to a rise in sea level. The model is based on Brotchie & Silvester (1969) and assumes an initial elastic thickness of 85 km, a final elastic thickness of 25 km, and a uniform (Maxwell) viscosity of  $1.6 \times 10^{21}$  Pa s. The flexure is expressed as a ratio,  $t/\tau$ , of 0.1, 0.5, 1.0, and 2.0, where  $t$  is the time since loading and  $\tau$  is the Maxwell relaxation time. The model shows that a sea-level rise rotates the original shelf such that there is an increase in subsidence in a seaward direction and uplift in a landward direction. The rotation can be expected to have a profound effect on the boundary between deposition and nondeposition and, in the case of a clastic margin, the fluvial profile supplying the sediment. The gray arrow indicates the direction of shoreline shift that results from lithosphere relaxation.

response to a fall. Unraveling this tectonic control from stratigraphic sequences, however, will be challenging, especially because other factors such as variations in sediment dynamics due, for example, to migrating deltas and shelf bypass could result in similar stratal geometries.

### 4.3. Dynamic Topography

Since the mid- to late 1970s, researchers have known that Earth's topography can be explained partly isostatically by either thickness or density variations in the crust and subcrustal mantle and partly dynamically by some form of density-driven convection in the mantle (e.g., McKenzie et al. 1974, Sclater et al. 1975, Cochran & Talwani 1977). Present-day dynamic topography can be inferred by removing the isostatic contribution of crustal and lithospheric structure [as defined, for example, by CRUST 5.0 (Mooney et al. 1998) and the cooling half-space or plate model] from Earth's topography. Such studies (Davies & Pribac 1993, Panasyuk & Hager 2000, Pari & Peltier 2000) show that large regions of North America, Eurasia, and Australia are characterized by dynamic topography "lows" of up to  $\sim 1.5$  km, suggesting cold mantle downwelling, whereas the Pacific, Africa, and Antarctica correlate with dynamic topography "highs" of up to  $\sim 1.5$  km, suggesting hot mantle upwelling. Dynamic topography can also be predicted from numerical models of mantle dynamics, using the velocity structure derived from seismic tomographic data as a proxy for mantle buoyancy (e.g., Hager 1984). The predicted and observed dynamic topographies derived this way are in general agreement (e.g., Hager 1984, Gurnis 1992, Ricard et al. 1993, Lithgow-Bertelloni & Silver 1998). Finally, dynamic topography in the geological past can be estimated on the basis of subduction and plate-motion history; it may also contribute to continental flooding (e.g., Gurnis 1992, Mitrovica et al. 1989, Liu et al. 2008) as well as large-scale erosion and sedimentation (Flowers et al. 2012, Zhang et al. 2012).

A difficulty with both these approaches to estimating dynamic topography involves removing the effects of isostasy. Most calculations of the nonisostatic topography from compilations of seismic refraction data (e.g., CRUST 2.0), for example, assume an Airy model, whereas numerical

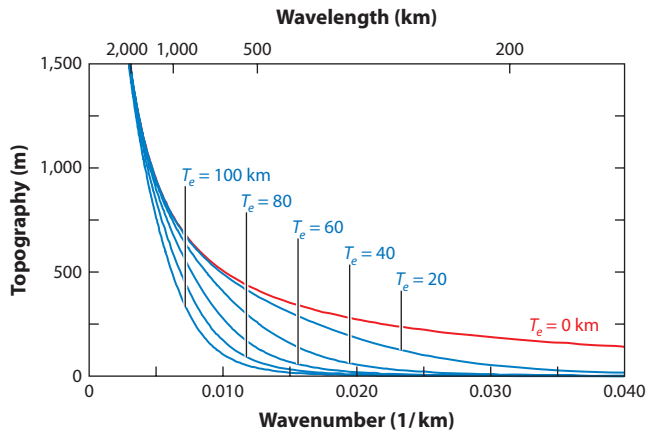


**Figure 11**

Plot of dynamic topography against wavelength for different values of the elastic thickness of the lithosphere,  $T_e$ . The dynamic topography has been calculated using the equations of McKenzie (2010), which are based on the deformation at the surface of a flexed elastic plate that overlies a convecting viscous half-space. The plot shows that the role of flexure in modifying the dynamic topography depends on wavelength. In the continents, where the mean  $T_e$  is 43.9 km, the flexural strength of the plate subdues the entire dynamic topography signal at wavelengths  $< \sim 250$  km. At longer wavelengths, the damping effect of the flexural strength decreases and the dynamic topography signal increases. At wavelengths  $> \sim 1,500$  km, flexure plays little or no role, and the dynamic topography approaches that expected for an Airy model.

model predictions generally consider the lithosphere as a deformable boundary layer that responds passively to motions in the underlying mantle. Both approaches ignore the strength of the lithosphere. We know, for example, that the topography, gravity anomaly, and crustal structure over surface loads such as oceanic islands and seamounts and ocean islands are well explained by a flexure model, and there is no reason to suppose that flexure will not also be important in the case of subsurface loads such as those associated with mantle convection, at least at certain wavelengths.

An elastic lithosphere will modify the surface topography due to motions in the underlying mantle as has been demonstrated by McKenzie et al. (1980), Watts & Daly (1981), and Zhong (2002), among others. High  $T_e$  subdues vertical motions in the sublithospheric mantle, whereas low  $T_e$  enhances them. The effects of mantle motions may, therefore, be more apparent in some tectonic settings (e.g., continental rifts, which have already been weakened) than in others. Flexure, however, is an isostatic model, so its contributions are limited by the wavelength of loading or unloading. At short wavelengths, for example, we would expect little or no response because the lithosphere will appear rigid, irrespective of its actual  $T_e$ . At long wavelengths, there would be a large response because the lithosphere will appear weak.

**Figure 11** shows the topography that would be expected for an elastic lithosphere at the surface of a viscous half-space, based on the recent study of McKenzie (2010). The figure shows that the amplitude of the deformation associated with convection increases as  $T_e$  decreases. In addition, the deformation decreases at short wavelengths and increases at long wavelengths, irrespective of the value of  $T_e$ .

The model in **Figure 11** assumes a uniform elastic plate and ignores the effect on motions in the underlying mantle of a lithosphere with a vertically stratified rheology. Even though this may not be important in the oceans, where the crust is thin, it will be important in the continents because the continents comprise more than one competent layer, for example, in the upper crust and upper mantle. Burov & Guillou-Frotier (2005) showed that a rheology where a strong, brittle

upper crust is mechanically decoupled from a strong, brittle mantle will drive the topography above, for example, a rising mantle plume to larger amplitudes and shorter wavelengths. This is because a buoyant mantle plume that impinges on the base of the lithosphere causes yielding in the brittle layers and ductile flow in the weak intervening layer, which results in thinning and strain localization. Therefore, despite the results illustrated in **Figure 11**, it is difficult to describe plume-lithosphere interactions in terms of a single cutoff wavelength below which flexure dampens the motions and above which the motions are enhanced.

An important question here is the influence that lithosphere relaxation may have on the topography associated with mantle convection. Most workers consider the timescales of mantle convection as long and of the order of tens to hundreds of millions of years. In this case, the lithosphere, once deformed, would already have undergone much of its relaxation and so it would behave essentially elastically. However, Müller et al. (2000) and DiCaprio et al. (2010) identified a dynamic topography “signal” in backstripped tectonic subsidence data from rifted continental margins that has an amplitude of up to several hundreds of meters and periods as short as a few million years. Therefore, it may be necessary to consider lithosphere relaxation when computing dynamic topography due, for example, to the vertical stresses that are generated by sinking slabs and rising plumes.

## 5. CONCLUSIONS

We draw the following conclusions from this review:

- The behavior of the lithosphere and how it responds to loading and unloading depends on its physical properties. A useful parameter that describes this behavior is the elastic thickness,  $T_e$ , which is a proxy for the strength of the lithosphere.
- Flexure studies show that  $T_e$  depends on both plate and load age. Young loads and old lithosphere yield the highest values (up to 80 km), whereas old loads and young lithosphere yield the lowest (<5 km). The range of elastic thickness values is smallest in the oceans (0–40 km) and greatest in the continents (0 to >70 km).
- $T_e$  is significantly less than the seismic thickness determined, for example, from controlled source seismology and teleseismic waves. If we consider the seismic thickness as reflecting the short-term response to loading and unloading and  $T_e$  as reflecting the long-term response, then on loading and unloading, the lithosphere must undergo some sort of stress relaxation as it thins from its short-term seismic to its long-term elastic thickness.
- The cause of this lithosphere relaxation is not fully understood, but it probably reflects some form of ductile and plastic flow in the mantle lithosphere of the type observed in data from experimental rock mechanics and predicted, for example, by the steady state creep laws for olivine.
- Multilayered viscoelastic plate models, in which viscosity is prescribed by the temperature structure, show that the relaxation is initially fast and then slows. This is explicable if, following a loading or unloading event, stress migrates upward from the warm, less viscous, lowermost part of the lithosphere to the cold, more viscous, uppermost part of the lithosphere, which has a high stress threshold and behaves essentially elastically on long timescales.
- $T_e$  data from the oceans can be generally fit by a multilayered viscoelastic model with an effective activation energy,  $Q = 120 \text{ kJ mol}^{-1}$ , sublithospheric mantle viscosity,  $\eta_{ref} = 10^{20} \text{ Pa s}$ , and power-law exponent  $n = 1$ .

- $T_c$  data from the continents require relatively high values of the effective activation energy (i.e.,  $200 < Q < 500 \text{ kJ mol}^{-1}$ ), if  $\eta_{ref} = 10^{20} \text{ Pa s}$ , and  $n = 1$ . These values of the effective activation energy are within the range of experimentally derived values for olivine.
- The global  $T_c$  data set can be reconciled if  $Q$  is high and oceanic mantle lithosphere is dominated by dislocation creep ( $n = 3.5$ ) while continental mantle lithosphere is dominated by diffusion creep ( $n = 1$ ). This is because increasing  $Q$  strengthens the mantle lithosphere, but dislocation creep weakens it. We cannot rule out the possibility, however, that a high  $Q$  and dislocation creep ( $n = 3.5$ ) dominate both plate settings and that the continental mantle lithosphere is significantly more hydrated than the oceanic mantle lithosphere.
- The relaxation time of old oceanic lithosphere is  $\sim 10^4$  yr, assuming a simple exponential decay for the subsidence. Comparable relaxation times have been deduced from glacial isostatic rebound studies. Relaxation times would be expected to vary spatially in the continents, however, and to be considerably shorter in regions of active tectonics, especially where the geotherm is elevated, and considerably longer in old, cold, cratonic regions.
- The phenomenon of lithosphere relaxation, which helps us understand how isostatic equilibrium is achieved on Earth, has a number of geological implications, including sedimentary basin evolution, sea-level change, and dynamic topography and should be considered within geodynamical models, including models for glacial isostatic adjustment.

## DISCLOSURE STATEMENT

The authors are not aware of any affiliations, memberships, funding, or financial holdings that might be perceived as affecting the objectivity of this review.

## ACKNOWLEDGMENTS

We thank an anonymous reviewer and Yukitoshi Fukahata for their helpful comments on an early draft of the paper. Tim Wright kindly provided a preprint of his recent paper on the geodetic and seismogenic determined elastic thickness. We thank the National Science Foundation (US-NSF 1114168) and Natural Environment Research Council (NE/1026839/1) for their support.

## LITERATURE CITED

- Ali MY, Watts AB. 2009. Subsidence history, gravity anomalies and flexure of the United Arab Emirates (UAE) foreland basin. *GeoArabia* 14:17–44
- Ali MY, Watts AB, Hill I. 2003. A seismic reflection profile study of lithospheric flexure in the vicinity of the Cape Verde islands. *J. Geophys. Res.* 108(B5):2239
- Allègre CJ, Dupre B, Lambret B, Richard P. 1981. The subcontinental versus suboceanic debate, I. Lead-neodymium-strontium isotopes in primary alkali basalts from a shield area: the Ahaggar volcanic suite. *Earth Planet. Sci. Lett.* 52:85–92
- Anderson DL, Minster JB. 1980. Seismic velocity, attenuation and rheology of the upper mantle. In *Coulomb Volume*, ed. C Allègre, pp. 13–22. Paris: Cent. Natl. Rech. Sci.
- Asaadi N, Ribe NM, Sobouti F. 2011. Inferring nonlinear mantle rheology from the shape of the Hawaiian swell. *Nature* 473:501–4
- Beaumont C. 1978. The evolution of sedimentary basins on a viscoelastic lithosphere: theory and examples. *Geophys. J. R. Astron. Soc.* 55:471–97
- Beaumont C. 1979. On rheological zonation of the lithosphere during flexure. *Tectonophysics* 59:347–65
- Beaumont C. 1981. Foreland basins. *Geophys. J. R. Astron. Soc.* 65:291–329
- Bloom A. 1967. Pleistocene shorelines: a new test of isostasy. *Geol. Soc. Am. Bull.* 78:1477–94

- Brotchie JF, Silvester R. 1969. On crustal flexure. *J. Geophys. Res.* 74:5240–45
- Burbank DW. 1992. Causes of recent Himalayan uplift deduced from deposited patterns in the Ganges basin. *Nature* 357:680–83
- Burov E, Guillou-Frottier L. 2005. The plume head-continental lithosphere interaction using a tectonically realistic formulation for the lithosphere. *Geophys. J. Int.* 161:469–90
- Catlos EJ, Harrison TM, Kohn MJ, Grove M, Ryerson FJ, et al. 2001. Geochronologic and thermobarometric constraints on the evolution of the Main Central Thrust, central Nepal Himalaya. *J. Geophys. Res.* 106:16177–204
- Chan GH-N, Waters DJ, Searle MP, Aitchison JC, Horstwood MSA, et al. 2009. Probing the basement of southern Tibet: evidence from crustal xenoliths entrained in a Miocene ultrapotassic dyke. *J. Geol. Soc. Lond.* 166:45–52
- Chappell J. 1974. Late Quaternary glacio- and hydro-isostasy, on a layered Earth. *Quat. Res.* 4:429–40
- Christensen NI. 1978. Ophiolites, seismic velocities and oceanic crustal structure. *Tectonophysics* 47:131–57
- Cochran JR, Talwani M. 1977. Free-air gravity anomalies in the world's oceans and their relationship to residual elevation. *Geophys. J. R. Astron. Soc.* 50:495–552
- Cohen SC, Darby DJ. 2003. Tectonic plate coupling and elastic thickness derived from the inversion of a steady state viscoelastic model using geodetic data: application to southern North Island New Zealand. *J. Geophys. Res.* 108(B3). doi: 10.1029/2001JB001687
- Collier J, Watts AB. 2001. Lithospheric response to volcanic loading by the Canary Islands: constraints from seismic reflection data in their flexural moats. *Geophys. J. Int.* 147:660–76
- Contreras-Reyes E, Grevemeyer I, Watts AB, Planert L, Flueh ER, Peirce C. 2010. Crustal intrusion beneath the Louisville hotspot track. *Earth Planet. Sci. Lett.* 289:323–33
- Courtney RC, Beaumont C. 1983. Thermally-activated creep and flexure of the oceanic lithosphere. *Nature* 305:201–4
- Davies GF, Pribac F. 1993. Mesozoic seafloor subsidence and the Darwin Rise, past and present. In *The Mesozoic Pacific: Geology, Tectonics, and Volcanism*, ed. S Pringle, *Geophys. Monogr.* 77:39–52. Washington, DC: AGU
- DiCaprio L, Müller RD, Gurnis M. 2010. A dynamic process for drowning carbonate reefs on the northeastern Australian margin. *Geology* 38:11–14
- Dixon JE, Dixon TH, Bell DR, Malservisi R. 2004. Lateral variation in upper mantle viscosity: role of water. *Earth Planet. Sci. Lett.* 222:451–67
- Flowers RM, Ault AK, Kelley SA, Zhang N, Zhong SJ. 2012. Epeirogeny or eustasy? Paleozoic-Mesozoic vertical motion of the North American continental interior from thermochronometry and implications for mantle dynamics. *Earth Planet. Sci. Lett.* 317–18:436–45
- Fluck P, Hyndman RD, Lowe C. 2003. Effective elastic thickness  $T_e$  of the lithosphere in western Canada. *J. Geophys. Res.* 108:2430. doi: 10.1029/2002JB002201
- Freedman AP, Parsons B. 1986. Seasat-derived gravity over the Musician seamounts. *J. Geophys. Res.* 91:8325–40
- Gaherty JB, Kato M, Jordan TH. 1999. Seismological structure of the upper mantle: a regional comparison of seismic layering. *Phys. Earth Planet. Inter.* 110:21–41
- Goetze C, Evans B. 1979. Stress and temperature in the bending lithosphere as constrained by experimental rock mechanics. *Geophys. J. R. Astron. Soc.* 59:463–78
- Grevemeyer I, Weigel W, Schussler S, Avedik F. 2001. Crustal and upper mantle structure and lithospheric flexure along the Society Island hotspot chain. *Geophys. J. Int.* 147:123–40
- Gurnis M. 1992. Rapid continental subsidence following the initiation and evolution of subduction. *Science* 255:1556–58
- Hager BH. 1984. Subducted slabs and the geoid: constraints on mantle rheology and flow. *J. Geophys. Res.* 89:6003–15
- Hartley R. 1995. *Isostasy of Africa: implications for the thermo-mechanical behaviour of the continental lithosphere*. PhD thesis. Oxford Univ., Oxford
- Hirth G, Kohlstedt DL. 2003. Rheology of the upper mantle and the mantle wedge. In *Inside the Subduction Factory*, ed. J Eiler, *Geophys. Monogr.* 138:83–105. Washington, DC: AGU

- Houseman G, Molnar P. 2001. Mechanisms of lithospheric rejuvenation associated with continental orogeny. *J. Geol. Soc. Lond.* 184:13–38
- Humphreys E, Hessler E, Dueker K, Farmer GL, Erslev E, Atwater T. 2003. How laramide-age hydration of North American lithosphere by the Farallon slab controlled subsequent activity in the western United States. *Int. Geol. Rev.* 45:575–95
- Hutton EWH, Syvitski JPM, Watts AB. 2013. Isostatic flexure of a finite slope due to sea-level rise and fall. *Comput. Geosci.* 53:58–68
- Iwasaki T, Matsu'ura M. 1982. Quasi-static crustal deformations due to a surface load: rheological structure of the Earth's crust and upper mantle. *J. Phys. Earth* 30:469–508
- Jackson J, McKenzie D, Priestley K, Emmerson B. 2008. New views on the structure and rheology of the lithosphere. *J. Geol. Soc. Lond.* 165:453–65
- Jordan TA, Watts AB. 2005. Gravity anomalies, flexure and the elastic thickness structure of the India-Eurasia collisional system. *Earth Planet. Sci. Lett.* 236:732–50
- Jordan TE. 1981. Thrust loads and foreland basin evolution, Cretaceous, western United States. *AAPG Bull.* 65:2506–20
- Kalnins LM, Watts AB. 2009. Spatial variations in effective elastic thickness in the western Pacific Ocean and their implications for Mesozoic volcanism. *Earth Planet. Sci. Lett.* 286:89–100
- Karato S, Wu P. 1993. Rheology of the upper mantle. *Science* 260:771–78
- Karner GD, Steckler MS, Thorne J. 1983. Long-term mechanical properties of the continental lithosphere. *Nature* 304:250–53
- Karner GD, Watts AB. 1983. Gravity anomalies and flexure of the lithosphere at mountain ranges. *J. Geophys. Res.* 88:10,449–77
- Kawakatsu H, Kumar P, Takei Y, Shinohara M, Kanazawa T, et al. 2009. Seismic evidence for sharp lithosphere-asthenosphere boundaries of oceanic plates. *Science* 324:499–502
- Latychev K, Mitrovica JX, Tamisiea ME, Tromp J. 2005. Influence of lithospheric thickness variations on 3-D crustal velocities due to glacial isostatic adjustment. *Geophys. Res. Lett.* 32(1). doi: 10.1029/2004GL021454
- Lin AT, Watts AB. 2002. Origin of the West Taiwan basin by orogenic loading and flexure of a rifted continental margin. *J. Geophys. Res.* 107:ETG2-1–19
- Lithgow-Bertelloni C, Silver PG. 1998. Dynamic topography, plate driving forces and the African superswell. *Nature* 395:269–72
- Liu L, Spasojevic S, Gurnis M. 2008. Reconstructing Farallon plate subduction beneath North America back to the Late Cretaceous. *Science* 322:934–37
- Luis JF, Neves MC. 2006. The isostatic compensation of the Azores Plateau: a 3D admittance and coherence analysis. *J. Volcanol. Geotherm. Res.* 156:10–22
- Lyon-Caen H, Molnar P. 1983. Constraints on the structure of the Himalaya from an analysis of gravity anomalies and a flexural model of the lithosphere. *J. Geophys. Res.* 88:8171–91
- Lyons SN, Sandwell DT, Smith WHF. 2000. Three-dimensional estimation of elastic thickness under the Louisville ridge. *J. Geophys. Res.* 105:13239–52
- Manea M, Manea VC, Kostoglodov V, Guzman-Speziale M. 2005. Elastic thickness of the oceanic lithosphere beneath Tehuantepec ridge. *Geofis. Int.* 44:157–68
- Mareschal JC, Jaupart C. 2004. Variations of surface heat flow and lithospheric thermal structure beneath the North American craton. *Earth Planet. Sci. Lett.* 223:65–77
- McKenzie D. 2010. The influence of dynamically supported topography on estimates of  $T_e$ . *Earth Planet. Sci. Lett.* 295:127–38
- McKenzie D, Fairhead D. 1997. Estimates of the effective elastic thickness of the continental lithosphere from Bouguer and free-air gravity anomalies. *J. Geophys. Res.* 102:27523–52
- McKenzie D, Jackson J, Priestley K. 2005. Thermal structure of oceanic and continental lithosphere. *Earth Planet. Sci. Lett.* 233:337–49
- McKenzie D, Watts AB, Parsons B, Roufousse M. 1980. Planform of mantle convection beneath the Pacific Ocean. *Nature* 288:442–46
- McKenzie DP, Roberts JM, Weiss NO. 1974. Convection in the Earth's mantle: towards a numerical simulation. *J. Fluid Mech.* 82:465–538

- Mei S, Suzuki AM, Kohlstedt DL, Dixon NA, Durham WB. 2010. Experimental constraints on the strength of the lithospheric mantle. *J. Geophys. Res.* 115(B8). doi: 10.1029/2009JB006873
- Minshull TA, Ishizuka O, Garcia-Castellanos D. 2010. Long-term growth and subsidence of Ascension Island: constraints on the rheology of young oceanic lithosphere. *Geophys. Res. Lett.* 37(23). doi: 10.1029/2010GL045112
- Minshull TA, Ishizuka O, Mitchell NC, Evangelidis C. 2003. Vertical motions and lithosphere rheology at Ascension Island. *Eos Trans. AGU* 84(46), Fall Meet. Suppl., Abstr. V11B-06
- Mitrovica JX, Beaumont C, Jarvis G. 1989. Tilting of continental interiors by the dynamical effects of subduction. *Tectonics* 8:1079-94
- Mooney WD, Laske G, Masters TG. 1998. CRUST 5.1: a global crustal model at  $5^\circ \times 5^\circ$ . *J. Geophys. Res.* 103:727-47
- Motagh M, Klotz J, Tavakoli F, Djamour Y, Arabi S, et al. 2006. Combination of precise leveling and InSAR data to constrain source parameters of the  $M_w = 6.5$ , 26 December 2003 Bam earthquake. *Pure Appl. Geophys.* 163:1-18
- Müller RD, Lim VSL, Isern AR. 2000. Late Tertiary tectonic subsidence on the northeast Australian passive margin: response to dynamic topography? *Mar. Geol.* 162:337-52
- Nishimura T, Thatcher W. 2003. Rheology of the lithosphere inferred from postseismic uplift following the 1959 Hebgen Lake earthquake. *J. Geophys. Res.* 108(B8). doi: 10.1029/2002JB002191
- Panasuk SV, Hager BH. 2000. Models of isostatic and dynamic topography, geoid anomalies and their uncertainties. *J. Geophys. Res.* 105:28199-209
- Pari G, Peltier WR. 2000. Subcontinental mantle dynamics: a further analysis based on the joint constraints of dynamic surface topography and free-air gravity. *J. Geophys. Res.* 105:5635-62
- Parker RL. 1972. The rapid calculation of potential anomalies. *Geophys. J. R. Astron. Soc.* 31:447-55
- Parsons BE, Sclater JG. 1977. An analysis of the variation of ocean floor bathymetry and heat flow with age. *J. Geophys. Res.* 82:803-27
- Pavlis NK, Holmes SA, Kenyon SC, Factor JK. 2008. An Earth gravitational model to degree 2160: EGM2008. *Geophys. Res. Abstr.* 10:EGU2008-A-01891
- Peltier WR. 2002. Global glacial isostatic adjustment: palaeogeodetic and space-geodetic tests of the ICE-4G (VM2) model. *J. Quat. Sci.* 17:491-510
- Peltier WR, Shennan I, Drummond R, Horton B. 2002. On the postglacial isostatic adjustment of the British Isles and the shallow viscoelastic structure of the Earth. *Geophys. J. Int.* 148:443-75
- Pérez-Gussinyé M, Lowry AR, Watts AB. 2007. Effective elastic thickness of South America and its implications for intracontinental deformation. *Geochem. Geophys. Geosyst.* 8:5009. doi: 10.1029/2006GC001511
- Pérez-Gussinyé M, Metois M, Fernandez M, Verges J, Fullea J, Lowry AR. 2009. Effective elastic thickness of Africa and its relationship to other proxies for lithospheric structure and surface tectonics. *Earth Planet. Sci. Lett.* 287:152-67
- Pérez-Gussinyé M, Watts AB. 2005. The long-term strength of Europe and its implications for plate-forming processes. *Nature* 436:381-84
- Pim J, Peirce C, Watts AB, Grevemeyer I, Krabbenhoef A. 2008. Crustal structure and origin of the Cape Verde Rise. *Earth Planet. Sci. Lett.* 272:422-28
- Podolefsky NS, Zhong SJ, McNamara AK. 2004. The anisotropic and rheological structure of the oceanic upper mantle from a simple model of plate shear. *Geophys. J. Int.* 158:287-296
- Pollitz FF. 2003. Transient rheology of the uppermost mantle beneath the Mojave Desert, California. *Earth Planet. Sci. Lett.* 215:89-104
- Priestley K, McKenzie D. 2006. The thermal structure of the lithosphere from shear velocities. *Earth Planet. Sci. Lett.* 244:285-301
- Quinlan GM, Beaumont C. 1984. Appalachian thrusting, lithospheric flexure and the Paleozoic stratigraphy of the eastern interior of North America. *Can. J. Earth Sci.* 21:973-96
- Rees BA, Detrick RS, Coakley BJ. 1993. Seismic stratigraphy of the Hawaiian flexural moat. *Geol. Soc. Am. Bull.* 105:189-205
- Ricard Y, Richards M, Lithgow-Bertelloni C, Le Stunff Y. 1993. A geodynamical model of mantle density heterogeneity. *J. Geophys. Res.* 98:21895-909

- Rychert CA, Fischer KM, Rondenay S. 2005. A sharp lithosphere-asthenosphere boundary imaged beneath eastern North America. *Nature* 436:542–45
- Sacek V, Ussami N. 2009. Reappraisal of the effective elastic thickness for the sub-Andes using 3-D finite element flexural modelling, gravity and geological constraints. *Geophys. J. Int.* 179:778–86
- Saltus RW, Thompson GA. 1995. Why is it downhill from Tonopah to Las Vegas? A case for mantle plume support of the high northern Basin and Range. *Tectonics* 14:1235–44
- Sandwell DT, Smith WHF. 1997. Marine gravity anomaly from Geosat and ERS-1 satellite altimetry. *J. Geophys. Res.* 102:10039–54
- Slater JG, Lawver LA, Parsons BE. 1975. Comparison of long wavelength residual elevation and free air gravity anomalies in the North Atlantic and possible implications for the thickness of the lithosphere plate. *J. Geophys. Res.* 80:1031–52
- Shapiro NM, Ritzwoller MH. 2002. Monte-Carlo inversion for a global shear-velocity model of the crust and upper mantle. *Geophys. J. Int.* 151:88–105
- Sheffels B, McNutt M. 1986. Role of subsurface loads and regional compensation in the isostatic balance of the Transverse Ranges, California: evidence for intracontinental subduction. *J. Geophys. Res.* 91:6419–31
- Sleep NH, Snell NS. 1976. Thermal contraction and flexure of mid-continent and Atlantic marginal basins. *Geophys. J. R. Astron. Soc.* 45:125–54
- Sloss LL, Scherer W. 1975. Geometry of sedimentary basins: applications to the Devonian of North America and Europe. *Geol. Soc. Am. Mem.* 142:71–88
- Stewart J, Watts AB. 1997. Gravity anomalies and spatial variations of flexural rigidity at mountain ranges. *J. Geophys. Res.* 102:5327–52
- Swain CJ, Kirby JF. 2006. An effective elastic thickness map of Australia from wavelet transforms of gravity and topography using Forsyth's method. *Geophys. Res. Lett.* 33(2). doi: 10.1029/2005GL025090
- Sweeney JF. 1977. Subsidence of the Sverdrup basin, Canadian Arctic Islands. *Geol. Soc. Am. Bull.* 88:41–48
- Tassara A, Swain C, Hackney R, Kirby J. 2006. Elastic thickness structure of South America estimated using wavelets and satellite-derived gravity data. *Earth Planet. Sci. Lett.* 253:17–36
- Tiwara VM, Mishra DC. 1999. Estimation of effective elastic thickness from gravity and topography data under the Deccan Volcanic Province, India. *Earth Planet. Sci. Lett.* 171:289–99
- Ussami N, Cogo de Sa N, Molina EC. 1993. Gravity map of Brazil. 2. Regional and residual isostatic anomalies and their correlation with major tectonic provinces. *J. Geophys. Res.* 98:2199–208
- van Hunen J, Zhong SJ, Shapiro NM, Ritzwoller MH. 2005. New evidence for dislocation creep from 3-D geodynamic modeling the Pacific upper mantle structure. *Earth Planet. Sci. Lett.* 238:146–55
- Vergnolle M, Pollitz F, Calais F. 2003. Constraints on the viscosity of the continental crust and mantle from GPS measurements and postseismic deformation models in western Mongolia. *J. Geophys. Res.* 108(B10). doi: 10.1029/2002JB002374
- Walcott RI. 1973. Structure of the Earth from glacio-isostatic rebound. *Annu. Rev. Earth Planet. Sci.* 1:15–38
- Wang Y, Mareschal J-C. 1999. Elastic thickness of the lithosphere in the Central Canadian Shield. *Geophys. Res. Lett.* 26:3033–36
- Watts AB. 2001. *Isostasy and Flexure of the Lithosphere*. Cambridge, UK: Cambridge Univ. Press. 458 pp.
- Watts AB, Bodine JH, Steckler MS. 1980. Observations of flexure and the state of stress in the oceanic lithosphere. *J. Geophys. Res.* 85:6369–76
- Watts AB, Daly SF. 1981. Long wavelength gravity and topography anomalies. *Annu. Rev. Earth Planet. Sci.* 9:415–48
- Watts AB, Ryan WBF. 1976. Flexure of the lithosphere and continental margin basins. *Tectonophysics* 36:25–44
- Watts AB, Zhong S. 2000. Observations of flexure and the rheology of oceanic lithosphere. *Geophys. J. Int.* 142:855–75
- Willett SD, Chapman DS, Neugebauer HJ. 1985. A thermo-mechanical model of continental lithosphere. *Nature* 314:520–23
- Wright TJ, Elliot J, Wang H, Ryder I. 2013. Earthquake cycle deformation and the Moho: implications for the rheology of continental lithosphere. *Tectonophysics*. In press
- Yamasaki T, Houseman GA. 2012. The crustal viscosity gradient measured from post-seismic deformation: a case study of the 1997 Manyi (Tibet) earthquake. *Earth Planet. Sci. Lett.* 351–352:105–14

- Zhang N, Zhong SJ, Flowers RM. 2012. Predicting and testing continental vertical motion histories since the Paleozoic. *Earth Planet. Sci. Lett.* 317–318:426–35
- Zheng Y, Arkani-Hamed J. 2002. Rigidity of the Atlantic oceanic lithosphere beneath New England seamounts. *Tectonophysics* 359:359–69
- Zhong S. 1997. Dynamics of crustal compensation and its influences on crustal isostasy. *J. Geophys. Res.* 102:15287–99
- Zhong S. 2002. Effects of lithosphere on the long-wavelength gravity anomalies and their implications for the formation of the Tharsis rise on Mars. *J. Geophys. Res.* 107(E7):8-1–13
- Zhong S, Paulson A, Wahr J. 2003. Three-dimensional finite element modelling of Earth's viscoelastic deformation: effects of lateral variations in lithospheric thickness. *Geophys. J. Int.* 155:679–95



# Contents

On Escalation <i>Geerat J. Vermeij</i> .....	1
The Meaning of Stromatolites <i>Tanja Bosak, Andrew H. Knoll, and Alexander P. Petroff</i> .....	21
The Anthropocene <i>William F. Ruddiman</i> .....	45
Global Cooling by Grassland Soils of the Geological Past and Near Future <i>Gregory J. Retallack</i> .....	69
Psychrophiles <i>Khawar S. Siddiqui, Timothy J. Williams, David Wilkins, Sheree Yau, Michelle A. Allen, Mark V. Brown, Federico M. Lauro, and Ricardo Cavicchioli</i> .....	87
Initiation and Evolution of Plate Tectonics on Earth: Theories and Observations <i>Jun Korenaga</i> .....	117
Experimental Dynamos and the Dynamics of Planetary Cores <i>Peter Olson</i> .....	153
Extracting Earth's Elastic Wave Response from Noise Measurements <i>Roel Snieder and Eric Larose</i> .....	183
Miller-Urey and Beyond: What Have We Learned About Prebiotic Organic Synthesis Reactions in the Past 60 Years? <i>Thomas M. McCollom</i> .....	207
The Science of Geoengineering <i>Ken Caldeira, Govindasamy Bala, and Long Cao</i> .....	231
Shock Events in the Solar System: The Message from Minerals in Terrestrial Planets and Asteroids <i>Philippe Gillet and Ahmed El Goresy</i> .....	257
The Fossil Record of Plant-Insect Dynamics <i>Conrad C. Labandeira and Ellen D. Currano</i> .....	287

The Betic-Rif Arc and Its Orogenic Hinterland: A Review <i>John P. Platt, Whitney M. Bebr, Katherine Jobanesen, and Jason R. Williams</i> .....	313
Assessing the Use of Archaeal Lipids as Marine Environmental Proxies <i>Ann Pearson and Anitra E. Ingalls</i> .....	359
Heat Flow, Heat Generation, and the Thermal State of the Lithosphere <i>Kevin P. Furlong and David S. Chapman</i> .....	385
The Isotopic Anatomies of Molecules and Minerals <i>John M. Eiler</i> .....	411
The Behavior of the Lithosphere on Seismic to Geologic Timescales <i>A.B. Watts, S.J. Zhong, and J. Hunter</i> .....	443
The Formation and Dynamics of Super-Earth Planets <i>Nader Haghighipour</i> .....	469
Kimberlite Volcanism <i>R.S.J. Sparks</i> .....	497
Differentiated Planetesimals and the Parent Bodies of Chondrites <i>Benjamin P. Weiss and Linda T. Elkins-Tanton</i> .....	529
Splendid and Seldom Isolated: The Paleobiogeography of Patagonia <i>Peter Wilf, N. Rubén Cúneo, Ignacio H. Escapa, Diego Pol, and Michael O. Woodburne</i> .....	561
Electrical Conductivity of Mantle Minerals: Role of Water in Conductivity Anomalies <i>Takashi Yoshino and Tomoo Katsura</i> .....	605
The Late Paleozoic Ice Age: An Evolving Paradigm <i>Isabel P. Montañez and Christopher J. Poulsen</i> .....	629
Composition and State of the Core <i>Kei Hirose, Stéphane Labrosse, and John Hernlund</i> .....	657
Enceladus: An Active Ice World in the Saturn System <i>John R. Spencer and Francis Nimmo</i> .....	693
Earth's Background Free Oscillations <i>Kiwamu Nishida</i> .....	719
Global Warming and Neotropical Rainforests: A Historical Perspective <i>Carlos Jaramillo and Andrés Cárdenas</i> .....	741
The Scotia Arc: Genesis, Evolution, Global Significance <i>Ian W.D. Dalziel, Lawrence A. Lawver, Ian O. Norton, and Lisa M. Gabagan</i> .....	767